
# Advances in modeling of fixed-abrasive processes

CIRP Annals - Manufacturing Technology 00 (2024) 1–26

Contents lists available at ScienceDirect

CIRP Annals - Manufacturing Technology

journal homepage: https://www.editorialmanager.com/CIRP/default.aspx

# Advances in modeling of fixed-abrasive processes

Peter Krajnik (2)[a], Konrad Wegener (1)[b], Thomas Bergs (2)[c], Albert J. Shih (1)[d,e]

[a] Chalmers University of Technology, Department of Industrial and Materials Science (IMS), Gothenburg, Sweden
[b] ETH Zürich, Institute of Machine Tools and Manufacturing (IWF), Zürich, Switzerland
[c] RWTH Aachen University, Manufacturing Technology Institute (MTI), Aachen, Germany
[d] University of Michigan, Department of Mechanical Engineering, Ann Arbor, MI, USA
[e] National Tsing Hua University, Department of Power Mechanical Engineering, Hsinchu, Taiwan

ARTICLE INFO

*Article history:*
Available online xxx

*Keywords:*
Grinding
Modeling
Simulation

ABSTRACT

Research over the last 70 years has led to a better understanding of fixed-abrasive machining processes. This knowledge is often expressed in the form of physical and empirical models that cover forces, power, specific energy, wheel/workpiece topography, wear, thermal aspects, cooling, dressing, and more. This paper first examines the established models that continue to constitute the fundamental knowledge base in fixed-abrasive technology. Special attention is given to geometry, kinematics, and thermomechanical modeling. Recent advances in process monitoring and big data analytics provide new opportunities to further strengthen the state of the art in modeling through data-driven approaches. In addition, examples on how models – implemented in simulation software – can be used to predict and optimize industrial operations have been demonstrated. This is illustrated by several use cases from real production, including bearing, creep-feed form, gear, camshaft, crankshaft, and centerless grinding, along with diamond-wheel truing.


## 1. Introduction

Machining with fixed abrasives remains one of the least-understood machining processes. This perception has been present since at least the 1950s, when investigations into its fundamental mechanics began to be published. Early grinding pioneer Tarasov wrote: *"grinding is such a complex process to analyze mathematically"* [17]. Decades later, new grinding models are being developed and established models are becoming ever more complex. Macro-scale quantities, such as process kinematics, are being integrated alongside micro-scale properties, such as wheel topography. More recently, in-process monitoring data has been integrated as a feedback into these models [34]. Modeling is a useful tool for overcoming the complexity that hinders process understanding. Here, the term *"modeling"* refers to the derivation of equations and functions that quantify the relationships within the process. The resulting *"model"* describes and quantifies the interrelation of input and output parameters in the process. Once developed, the model is used in trials to simulate the process behavior, typically through a computer program. Such *"simulation"* with the model provides predictive insights about the process.

Models can be broadly categorized as (i) physical or (ii) empirical, as defined in previous CIRP keynote papers, published in 1992 [255] and 2006 [44]. Physical models rely strictly on first principles and physical laws. In classical grinding research, an essential part of physical modeling is the application of fundamental mechanics, such as the proportionality of force to specific energy and cross-sectional chip area [17]. Such underlying laws have general validity and lead to a better understanding of fundamental process mechanics. However, many analytical problems in grinding cannot be solved with general validity, so approximations are obtained through numerical calculations. This constitutes numerical modeling, which is ever-increasing due to the wide availability of computers and software, which allow for modeling of complex processes [113]. For example, the finite element method (FEM) is used extensively to solve partial differential equations by a series of approximations that satisfy the governing equation and boundary conditions within a small region of a grinding zone/contact interface [134]. In this context, a semi-analytical model uses theoretical principles as a foundation and then couples it with numerical methods to deal with the complexities of the process [277]. Empirical models are developed through experimentation on the actual grinding system or its analog. This approach treats the process as a "black box" and focuses on data analysis, including fitting models to data and making model inferences based on data. Examples of empirical models are numerous, including regression analysis [76,166], Monte Carlo method [291], Bayesian data analysis [195], exploratory data analysis [253], and artificial neural networks (ANN) [275] – a cornerstone of machine learning (ML). Here, ML is considered a subset of artificial intelligence (AI), which is based on

*E-mail address:* krajnik@chalmers.se (P. Krajnik).

https://doi.org/10.1016/j.cirp.2024.05.001

supervised, unsupervised, and deep learning from data [279]. Such data-driven modeling now plays a pivotal role in empirical efforts. One drawback of empirical models is their limited ability to accurately predict outcomes beyond the range of given experimental data, as these models are built on interpolation of observed values rather than on the underlying physical principles.

This keynote paper aims to demonstrate how modeling can lead to accurate predictions of fixed-abrasive processes. To this end, a variety of physical and empirical models that describe key process aspects – such as specific energy/forces, wheel wear, temperatures, thermal damage and surface roughness – are described. While the focus is on the modeling of grinding and dressing processes, the principles extend to other fixed-abrasive processes, such as honing [33,48,106] and superfinishing [155,156], due to similar underlying mechanisms. Modeling on a macro-scale extends to a micro-scale, with significant advancements being made in both domains [60,149,150,242]. Abrasive machining is used to finish precision components, mainly in metals, but also in ceramics, composites, and other functional materials. For example, modeling has advanced the understanding of the kinematics in cup-wheel grinding of silicon wafers [137] and kinematics in contour-grinding of PVD-coated optical molds [129]. Similarly, models of ceramic grinding can quantify the undeformed chip thickness [4,281] and predict surface integrity [62].

The key sections of the paper (Fig. 1) are as follows: Section 2 begins with a brief review of the evolution of fundamental models that describe grinding mechanisms. It then continues with a discussion on the fundamentals of geometry and kinematics for a variety of fixed-abrasive processes, covering aspects of wheel truing and dressing as well as wheel and workpiece topography. Section 3 discusses thermomechanical modeling of grinding based on physical laws, including material removal, wear, thermal aspects and fluid flow (effect of grinding fluid). The process-machine interactions are discussed only briefly because modeling of chatter is considered outside the scope of this work. Section 4 addresses emerging data-driven modeling, which aids empirical predictions of wear, grinding burn and surface roughness. Section 5 discusses the use of simulation models that have impacted real production in the bearing, automotive, and aerospace sectors.

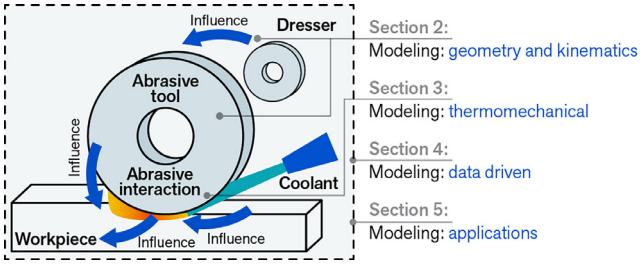


**Fig. 1.** Systemic approach to modeling of fixed-abrasive processes.

## 2. Modeling – geometry and kinematics

### 2.1. Evolution of grinding models

Early grinding models were derived from metal-cutting models [208]. For example, Merchant proposed a system of forces acting on an abrasive grit where the radial and tangential forces are in equilibrium with the normal and frictional forces [17]. However, the situation is complicated by the unknown three-dimensional grit geometry and rake angle, which is in contrast to the geometrically defined cutting edge in two-dimensional orthogonal cutting. Two distinctive characteristics of grinding compared to metal cutting are: (i) the magnitude of shearing; and (ii) the relatively large increase in specific energy with decrease in undeformed chip thickness, known as the size effect [16]. The specific energy is a fundamental process parameter, defined as the energy required to remove unit volume of material [206]. The original investigation of the specific energy was purely experimental, from surface-grinding tests at the Timken Company. A dynamometer mounted to a surface grinder measured the normal $F_n$ and tangential $F_t$ forces for various depths of cut $a_e$, workpiece speeds $v_w$, wheel speeds $v_s$, and grinding widths $b_D$. Based on the results, the specific energy was established as:

$$e_c = \frac{F_t \cdot v_s}{v_w \cdot a_e \cdot b_D} = \frac{P}{Q_w} \tag{1}$$

where the numerator is the grinding power $P$, and the denominator is the volumetric material removal rate $Q_w$. The specific energy can be derived from the power (or force) measurements and grinding conditions, and it can be associated with the three distinct abrasive mechanisms of sliding, plowing, and chip formation. Therefore, it quantifies the efficiency of material removal. The same authors [16] further defined the geometric contact length:

$$l_g = \sqrt{a_e \cdot d_e} \tag{2}$$

where $d_e$ is the equivalent wheel diameter calculated as $d_e = d_w \cdot d_s/(d_w \pm d_s) = d_s/(1 \pm d_s/d_w)$, where the plus sign is for outside-diameter (OD) grinding and the minus sign for internal-diameter (ID) grinding, and $d_e = d_s$ for surface grinding (as $d_w \to \infty$). For practical purposes, there is no need to distinguish between the $l_g$ and the kinematic-contact length $l_k$ as the difference is extremely small for typical $v_w$ and $v_s$ values. The other fundamental parameter, derived in 1952 [16], is the maximum undeformed chip thickness, or the "grit depth of cut", defined as:

$$h_m = \sqrt{\frac{4}{C \cdot r}\left(\frac{v_w}{v_s}\right)\sqrt{\frac{a_e}{d_e}}} \tag{3}$$

where $C$ is the number of cutting points per unit area (cutting-point density) and $r$ is the chip-shape ratio (ratio of chip width to chip thickness). Quantifying these two wheel-topography parameters has proven to be difficult.

The role of chip thickness in grinding was first investigated already in 1914 [7] by George I. Alden, who co-founded the Norton Company. His work is considered the first grinding-modeling paper. Alden derived a mathematical relationship for the "grit depth of cut" as a function of the grinding conditions for cylindrical OD grinding (Fig. 2). This model translates to maximum undeformed chip thickness as $h_m = (2/N)(v_w/v_s)\sqrt{a_e/d_e}$ using established symbols (as per [202]), where $N$ is the number of cutting points per unit length of circumference. Note that the inverse of $N$ corresponds to the cutting-point spacing $L$.

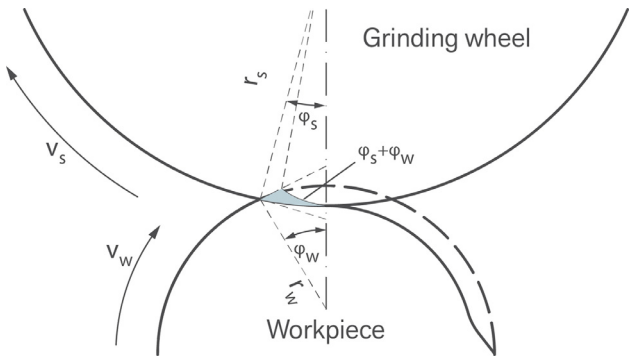


**Fig. 2.** Geometry and kinematics of cylindrical OD grinding according to Alden (adapted from [7]).

In 1943, the $h_m = 2L(v_w/v_s)\sqrt{a_e/d_e}$ model was adopted in Germany [216], see Fig. 3. Researchers identified the importance and the role of geometrical ($a_e$, $d_e$) and kinematical ($v_w$, $v_s$) parameters (and their ratios) on process mechanics [223].

The dimensionless parameter that accounts for the process geometry and kinematics $(v_w/v_s)\sqrt{a_e/d_e}$ was termed chip-thickness

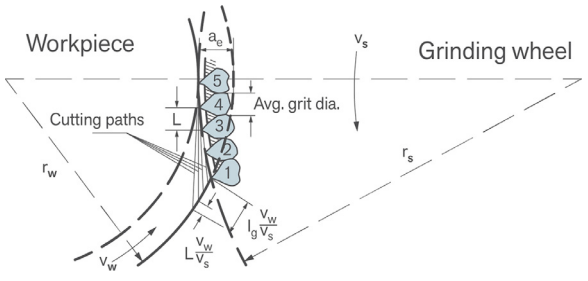


**Fig. 3.** Illustration of material removal by simultaneous engagement of several abrasive grits during cylindrical OD grinding (adapted from [216]).

coefficient [274]. Peklenik postulated that the cutting points are not equally spaced (i.e., $L \neq$const.) and do not protrude uniformly. This leads to stochastic, topography-dependent, models that are largely used today. The number of active cutting points depends on both the topography of the wheel (grit protrusion), and the grinding conditions. This was studied in detail by [153]. The analysis of the "static" cutting-point density, as determined from measurements of the wheel topography, was integrated into the "dynamic" cutting-point density, $C_{dyn}$, which also takes into account geometry and kinematics. To further investigate this, Tigerström [254] developed a method to measure $C_{dyn}$ and then correlate it against the dimensionless parameter $(v_w/v_s)\sqrt{a_e/d_e}$. Malkin labeled this quantity the infeed angle $\varepsilon$, representing the material flow relative to a contact point on the periphery of the wheel [202].

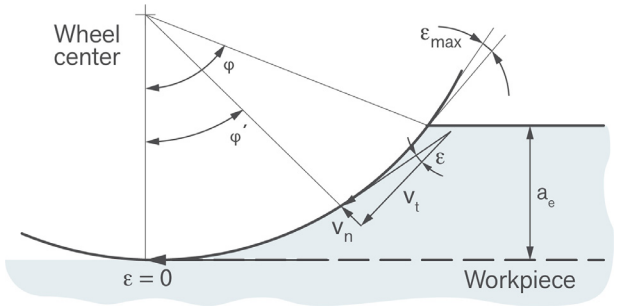


**Fig. 4.** Illustration of infeed angle of material flow relative to a cutting point on the wheel periphery (adapted from [202]).

As a contact point on the grinding wheel moves through the grinding zone, its motion will intersect with that of the moving workpiece, which is a necessary condition for cutting. The level of interference at any point along the cutting path is determined by the infeed angle between the normal $v_n$ and tangential $v_t$ components of the relative velocity vector, as shown in Fig. 4. The infeed angle decreases from the top of the cutting path, where the maximum value of the infeed angle can be calculated as [273]:

$$\tan \varepsilon_{max} = 2\left(\frac{v_w}{v_s}\right)\sqrt{\frac{a_e}{d_e}} \tag{4}$$

towards $\varepsilon = 0$ at the bottom of the cutting path; with the average value $\bar{\varepsilon}$ halfway through the contact length being equal to $\tan\bar{\varepsilon} = (v_w/v_s)\sqrt{a_e/d_e}$ [202] because of the extremely small values for $\varepsilon$. It was not until 2008 that this dimensionless quantity was given a new name: the aggressiveness number, *Aggr*, quantified as [18]:

$$Aggr = \left(\frac{v_w}{v_s}\right)\sqrt{\frac{a_e}{d_e}} \tag{5}$$

However, in 1974, despite the prevalent use of this dimensionless parameter, the $(v_w/v_s)\sqrt{a_e/d_e}$ was replaced by a dimensional parameter – the equivalent chip thickness [246]:

$$h_{eq} = v_w \cdot a_e/v_s = Q'_w/v_s \tag{6}$$

The parameter $h_{eq}$ can be interpreted as the thickness of a continuous ribbon of material being removed from a ground workpiece flowing away along the grinding wheel at the wheel speed $v_s$ and the volume of which is equal to that of the material removal $V_w$ during the same time period. Unfortunately, $h_{eq}$ ignores the contact length. This limitation is illustrated in Fig. 5, where the correlation of surface finish with *Aggr* (Fig. 5b) is significantly better than with $h_{eq}$ (Fig. 5a), because *Aggr* considers contact length.

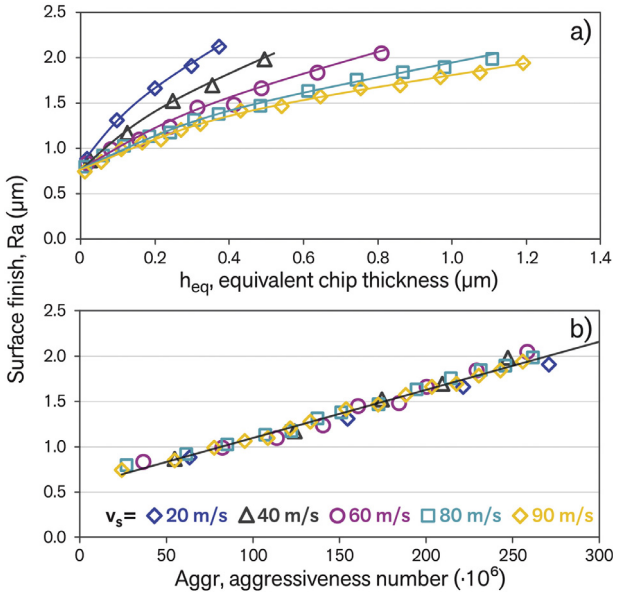


**Fig. 5.** Surface finish results charted over $h_{eq}$ and *Aggr* (data from [214]).

The introduction of equivalent chip thickness led to empirical curve-fitting, such as $Ra = R_1 {h_{eq}}^r$ and $Q'_w = Q_1 {h_{eq}}^q$ [246]. Based on this, a large number of empirical models were reduced to "basic models" [255], such as for maximum undeformed chip thickness and total-height surface roughness parameter $R_t$:

$$h_m = C_s\left(\frac{v_w}{v_s}\right)^{e_1}(a_e)^{\frac{e_1}{2}}\left(\frac{1}{d_e}\right)^{\frac{e_1}{2}} \tag{7}$$

$$R_t = C_s C_w\left(\frac{v_w}{v_s}\right)^{e_1}(a_e)^{e_2}\left(\frac{1}{d_e}\right)^{-e_3} \tag{8}$$

where $C_s$ is a constant for a specific grinding wheel, $C_w$ is a constant for a given workpiece, and $e_1$, $e_2$, and $e_3$ are exponents that must be experimentally determined for a given wheel-workpiece combination. The practical application of such empirical models can be time-consuming due to the identification of unknown parameters and is nowadays seldom used.

### 2.2. Dimensionless parameters

Considering that the dimensionless quantity $(v_w/v_s)\sqrt{a_e/d_e}$ (i) has been utilized in various models since 1914 [7], (ii) is featured in empirical "basic" models [255], and (iii) is of greater practical utility than $h_{eq}$, it is explored in greater detail here.

The fundamental definition of aggressiveness for any abrasive process (tool-workpiece contact) is simply the ratio of the normal component $v_n$ and the tangential component $v_t$ of the relative-velocity vector (shown in Fig. 4) at a contact point [89]:

$$Aggr^* = \frac{v_n}{v_t} = \frac{\vec{v}\cdot\vec{n}}{\sqrt{\vec{v}\cdot\vec{v} - (\vec{v}\cdot\vec{n})^2}} \tag{9}$$

Please cite this article as: P. Krajnik et al., Advances in modeling of fixed-abrasive processes, CIRP Annals - Manufacturing Technology (2024), https://doi.org/10.1016/j.cirp.2024.05.001

This fundamental parameter is termed point-aggressiveness $Aggr^*$. The process geometry is captured by the vector field of surface normal $\vec{n}$ at a contact point. The process kinematics is captured by the vector field of relative velocity $\vec{v}$. The theory of aggressiveness can be applied to any abrasive process where the process geometry ($\vec{n}$) and kinematics ($v_n$, $v_t$) are analytically described for an arbitrary contact point. From the mechanics perspective, the shear at any point in the abrasive contact can be expressed as $\tau = e_c \cdot Aggr^*$. This is consistent with the model for tangential force [17], which is proportional to specific energy and cross-sectional chip area $A_{ch}$ (where $A_{ch} = Aggr^*/C$).

The simplified quantity needed for optimization of grinding and dressing operations is the aggressiveness number $Aggr$ (Eq. (5)), which is the average point aggressiveness ($Aggr^*$). Formulas to calculate $Aggr$ in grinding operations are given in [20]. The application of $Aggr$ to optimize complex processes has to date included camshaft [163] and crankshaft grinding [91], saw-tip grinding [19], flute grinding [88], double-disc grinding [85], diamond-wheel truing [86] and face grinding [257,258].

The $Aggr^*$ or $Aggr$ numbers do not incorporate wheel-topography parameters. Nevertheless, in cases where wheel topography needs to be included, $Aggr^*$ can be replaced with $h_m$ by adding the $C$ and $r$ parameters, such as $h_m = \sqrt{4/(C \cdot r)Aggr^*}$.

### 2.3. Kinematic simulation

To conduct any grinding simulation, it is essential to model the kinematics of the wheel and workpiece bodies that move relative to each other. Grinding involves the interference of the two surfaces, both of which have a complex and time-dependent topography. Transforming the movement of the bodies into the relative movement of the contact points poses a significant challenge. The wheel comprises grits and pores, while the workpiece consists of long scratches that are quantified via various roughness parameters (discussed in Section 2.5). Therefore, a considerable amount of geometric data must be considered. The surface descriptions and kinematics, however, are closely interrelated, regardless of whether the interaction is described analytically or by field equations. After each time step, the interactions between each relevant grit and all relevant workpiece planes are calculated based on the current and previous tool positions, as shown in Fig. 6.

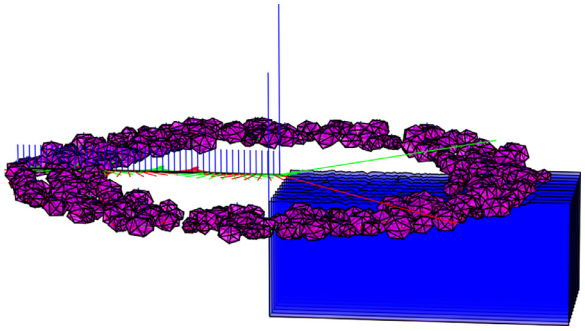

**Fig. 6.** Simulation of face-grinding kinematics in iBRUS software (ETH Zürich), where the wheel's grits are depicted as 3D meshes (purple) and the workpiece is discretized as a stack of 2D planes (blue). The coordinate axes represent the wheel's position and orientation with respect to time.

This concept introduces a generalized kinematics framework that facilitates the description of any fixed-abrasive process, for example diamond-wire sawing, abrasive-disc cutting, glass grinding, rail grinding, and core drilling with an abrasive tool.

### 2.4. Wheel truing, dressing, and topography

At the system level, grinding needs to be treated as a process chain shown in Fig. 7. The goal is to predict the outcome of grinding

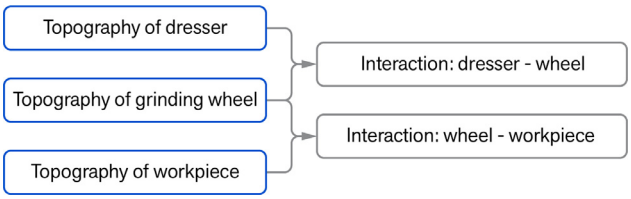


**Fig. 7.** System interactions in grinding.

by accounting for the contributions of interacting abrasive subsystems – or, inversely, to deduce the input parameters required to obtain the desired grinding results. This requires also modeling the interaction between the workpiece and the grinding wheel, as well as the interaction between the dresser and the grinding wheel – while identifying the necessary process windows and the topography of the grinding wheel. For example, [103] developed a kinematic model for rotary dressing that considered the stochastic topography of the grinding wheel as well as the topography of the dresser. The model also included material removal. These aspects were integrated in MATLAB.

Due to grinding-wheel wear, models must be capable of accommodating the transient grinding-wheel topography (e.g., wear) as work material is removed. A 3D surface is typically characterized by measurements taken with a microscope capable of mapping the 3D topography. Different descriptors are used to characterize this complex surface: (i) stochastic parameters, such as the Abbott-Firestone curve, or (ii) statistical data, such as the moments of height distribution. Based on the derived descriptors of the surface, the surface topography can be reconstructed. This requires additional information, which can be obtained from the geometry and positioning of abrasive grits with their stochastic shape, orientation, and density. The wheel surface can be digitally recreated by scanning real grits and stochastically placing them on the cylindrical reference surface by randomly rotating them about the normal to the reference plane [276]. For example, a grinding wheel topography was created by randomly selecting the diamond-grit morphology shown in Fig. 8. based on a normal distribution of the shape parameter and size [230]. The grits were positioned in a defined pattern with random rotation. The same morphology variable was used, but wear and/or dressing effect was added to represent shape change [205].

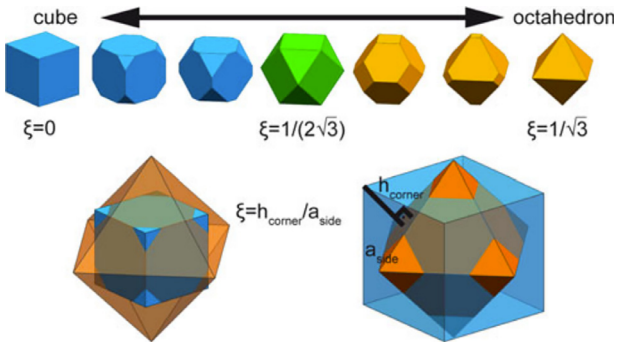


**Fig. 8.** Morphology of diamond hexa-octahedrons with the grit-shape variable for randomization [261].

The (macroscopic) wheel shape and the (microscopic) grinding-wheel topography are created by truing and dressing. Truing involves making the wheel round. It sometimes also involves putting a specific shape/profile into the wheel. Dressing involves creating a specific topography on the wheel, usually to achieve the desired grinding performance [202].

Malkin conducted a fundamental study of rotary-plunge dressing [203], focusing primarily on experimental analysis. The

parameters used were the dressing speed ratio $q_d = v_r/v_s$ (where $v_r$ is the dresser speed and $v_s$ is the wheel speed), the dressing direction (uni-directional or anti-directional), and the equivalent dresser infeed $a_r$. The dressing process was assessed based on specific dressing energy and surface roughness across different speed ratios and infeeds. For this, Malkin introduced the interference angle, $\delta$, which describes the angle at which the diamonds impact the wheel's periphery:

$$\delta = \tan^{-1}\left(\frac{a_r}{\pi d_s |1 - q_d|}\right) \quad (10)$$

where $d_s$ is the grinding wheel diameter. This model, however, does not account for the contact length between the dresser and the grinding wheel. Nevertheless, a good correlation between the specific dressing energy and the interference angle was obtained. It was also found that a larger $\delta$ (i.e. coarser dressing) results in lower grinding forces and produces rougher surface finishes. Brinksmeier introduced the collision number $i_d$ [45] to quantify interactions between the diamonds on a traverse dresser and the grits on the grinding wheel. In the context of traverse dressing, the collision number is proportional to $U_d|1 - q_d|$, where $U_d$ is the dressing overlap ratio. The collision number captures a complex interplay of factors, including dressing geometry and kinematics, the contact length, the size of grits on the grinding wheel and the dresser, and the number of diamond points per unit area of the dresser. A larger $\delta$ [203] and $i_d$ [45] both lead to higher abrasive grit or bond fracture and less grit dulling, resulting in lower specific grinding energies. Linke expanded the collision number model [183] by incorporating time-dependency and using acoustic emission (AE) to monitor the dressing process. The collision number showed a good correlation with the root mean square (RMS) value of the AE signal. Further research quantified the topographies of dressers and grinding wheels in terms of grit size and protrusion probabilities [247]. The determination of contact length required experimental calibration to account for the deflection in the abrasive contact. Discrete element method (DEM) was used for modeling these interactions. Most recently, the dressing aggressiveness number $Aggr_D$ was used to analytically model both traverse [191] and plunge-roll rotary dressing [21], combining the various dressing parameters into a single dimensionless parameter. Advances in wheel conditioning have been reviewed in [271]. It concluded that modeling of the dressing process is difficult due to: (i) the undefined cutting edges with complex grit morphology, (ii) the distribution, and (iii) the transient wear. Since then, various new approaches for modeling grinding wheel topography and dressing have been reported.

The typical distribution of grits on a grinding wheel is irregular, non-deterministic, and subject to changes over time due to wear. Therefore, active grits are not only randomly distributed, but their number and shape change during the process. A grit density function was introduced in [52] to describe the distribution of all active grits on the wheel, considering the total grinding force as the superposition of all engaging active single-grit forces. Analysis of wheel topography is critical for incorporating microscopic process effects. One method for analyzing grinding wheel topography involved using digital image processing and structured light microscopy [133]. Although not a modeling technique, it enabled 3D mapping of the wheel surface, which facilitated grit recognition after data processing and smoothing. This analysis provided information on grit size and rake angle distribution for the grits, allowing for the characterization of wheel-surface properties independent of process-specific parameters. A similar grinding-wheel surface reconstruction using measured data and a moving-average model to improve accuracy was described in [58]. The motion-trajectory equations for abrasive grits were established based on grinding kinematics. A model to represent grinding-wheel topography was proposed by introducing the degree of grit protrusion and grit-protrusion area, combined with topography parameters representing grit size and cutting-point spacing [186]. A neural network was utilized to predict wheel topography based on AE signals and feature extraction techniques

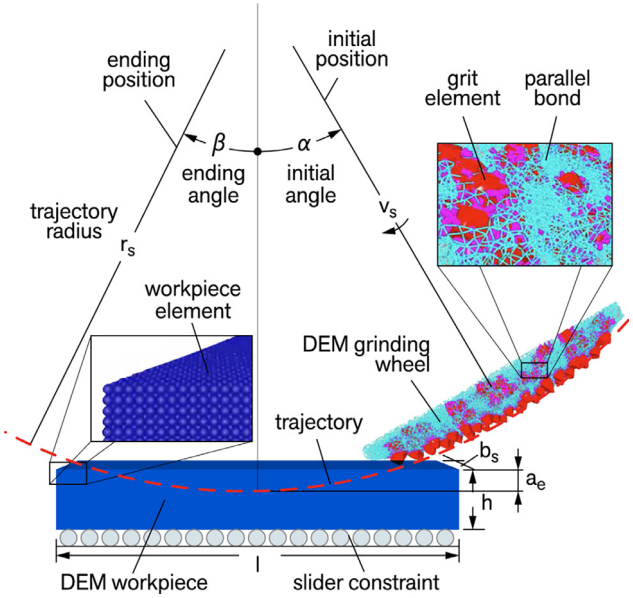


**Fig. 9.** Illustration of a DEM simulation [179].

[64]. Confocal microscopy was applied to measure the grinding wheel profile [290]. DEM was also utilized to model wheel topography to study, for example, wheel load bearing [179], as illustrated in Fig. 9. Similarly, a bonding bridge between grits was introduced to represent the bond and load-bearing capacity [215].

### 2.5. Workpiece topography

The first order workpiece deviations include flatness and roundness, which can originate from machine kinematic errors, improper clamping, thermal expansion, etc. Models addressing shape deviations often use multi-scale approaches to describe the global effects of local changes. Thermal-load effects in internal traverse grinding were modeled by combining thermomechanically coupled FE models and kinematic simulation [38]. Shape deviations were modeled by combining FEM with an experimentally obtained spindle-compliance response [74]. Workpiece distortion [241] was investigated with respect to thermally and mechanically induced residual stress in profile grinding. The impact of assembly errors on form deviation were investigated in gear profile-grinding machines [79].

Waviness parameters are derived from the surface profile after form deviation is reduced and high-frequency waveforms are filtered out. Because waviness can stem from forced vibrations (e.g., wheel imbalance/eccentricity, spindle runout), self-excited vibration, and periodical machine compliance, prediction of waviness requires models to consider specific sources of waviness. This often necessitates considering multiple scales [68]. The pre-existing workpiece waviness from previous machining operations was considered when modeling the grinding system response and waviness removal effectiveness [148]. Forced oscillations, acceleration, and audio measurements were measured to detect wheel eccentricity in a model that used a scallop-profile of workpiece waviness to predict the final scallop-shape profile [22].

The abrasive-grit tool path imparts marks on the workpiece from the plowing and cutting interactions, which produce a kinematic roughness. Various kinematic model-based approaches for calculating these parameters have been published. Grinding marks were analyzed based on surface function, typically considering spatial period and amplitude. The height of kinematic traces in conventional grinding [115] was modeled, while [56] adapted their model to account for the grinding marks on spherical and aspherical surfaces. [266] proposed a model for ball-end grinding of spherical surfaces. Numerous models have been developed for

Please cite this article as: P. Krajnik et al., Advances in modeling of fixed-abrasive processes, CIRP Annals - Manufacturing Technology (2024), https://doi.org/10.1016/j.cirp.2024.05.001

analyzing grinding marks in wafer grinding [54,138,288], while [219,289] modeled the kinematic roughness in parallel grinding and [226] developed a model to minimize error in optical-component grinding.

As previously mentioned, surface roughness is a vital quality requirement and key output of the grinding process. Its prediction is crucial [197]. The surface-roughness profile – filtered by form, waviness, and kinematic roughness – results in a high-frequency-spectrum profile that was generated by the interaction of the workpiece and the stochastically distributed grits. In a study by Peklenik published in 1964, the grinding process was treated as a linear transfer system with random inputs [224]. He postulated that wheel topographies are statistically independent, noting that the outputs – surface roughness (and wheel wear) – appear as stationary random processes that could be described in terms of averages and correlation functions. Sixty years later, the treatment of the correlation between wheel topography and surface roughness in probabilistic terms is still omnipresent. For example, a stochastic surface-roughness model was developed, where the resulting arithmetic-mean surface profile is directly calculated from the grooves generated during grit engagements, regardless of whether a grit is plowing or cutting [181]. A similar approach was applied to grinding with electroplated wheels [228], where a non-Gaussian wheel topography was generated using a numerical model – adopting a grit-distribution model that randomized grit size, protrusion height, and spacing while maintaining a uniform cutting-point density throughout the wheel. By integrating process kinematics, surface roughness could be predicted – constrained by the assumption that grits have a spherical shape. Another model for the prediction of surface roughness, based on probability-density functions for the undeformed chip thickness, considered elasto-plastic material behavior [251].

Surface texture profile and/or areal parameters are the main output quantities for almost all surface-roughness models. The primary differences between the models lie in their application to ductile or brittle materials and the material-removal phenomena: ductile removal (via elastic recovery, plowing and chip formation) or brittle removal (via elastic recovery and brittle fracture). [220] gave an overview of the extensive number of models available in the literature. Models focusing primarily on brittle-material behavior are found in [217,250, 292].

A model for predicting the impact of wheel topography on surface roughness in tool grinding was made by [81]. The topography that results from the overlay of kinematic paths while using ultrasonic excitation is positioned between micro-roughness and kinematic roughness. Several models were proposed for evaluating the impact of ultrasonic excitation on this topography [227]. The bearing ratio (Abbott-Firestone) curve is the cumulative density function of the profile and is often used to characterize grinding wheel topographies. Theoretically, it is also suitable for characterizing workpiece topography, as shown in [55]. This approach is sometimes used when modeling honing processes [102,106,107]. In theory, whenever roughness of a profile or surface is evaluated, the bearing-ratio curve can be derived, and related parameters may be used for surface comparison.

From a theoretical modeling perspective, it is possible to predict surface roughness by describing how abrasive cutting points kinematically interact with the workpiece. [280] derived a model for the total-height surface roughness – $R_t = {h_m}^{4/3}/{a_e}^{1/3}$ – which already accounted for wheel topography, since their expression for $h_m$ included parameters of $C$ and $r$. Malkin and Guo derived a similar basic model of an ideal ground surface profile, assuming uniform cutting-point spacing $L$ and no wear [202]:

$$R_t = \frac{1}{4}\left(\frac{v_w L}{v_s {d_s}^{1/2}}\right)^2 \tag{11}$$

These basic models imply that surface roughness mainly depends on the speed ratio $v_w/v_s$ and the spacing $L$, less on the wheel diameter $d_s$, and not at all on the depth of cut. However, this ideal surface roughness is far from roughness values obtained in production grinding, which suggests the necessity to account for real wheel topography (including dressing), height differences between the tips of the active grits, and wear (e.g., grit dulling).

## 3. Modeling – thermomechanical

### 3.1. Thermomechanical modeling framework

Predicting grinding outputs solely through models of geometry and kinematics is challenging due to the interconnected and non-stationary nature of the process. Thermomechanical modeling commences with the grinding wheel, defining the grit-workpiece contact, material removal, and thermal aspects of the process. Grinding kinematics is a necessary component of thermomechanical modeling, as it involves the relative motion between the grinding wheel and the workpiece (see Fig. 6). This must also take into account the potential impact of machine vibrations. In order to establish a process signature (characterizing the impact of a process on the work material [152]), the geometry and topography of the workpiece must be inputted. An ideal surface is typically used as a starting point, however, the contact with the grinding wheel inevitably leaves abrasive traces on the workpiece, with a certain surface roughness as an output. In addition, the effects of the fluid flow, phenomena of wear and heat release must also be included. An overview is shown in Fig. 10, which gives a more comprehensive understanding of the scope of the thermomechanical modules being discussed in this section.

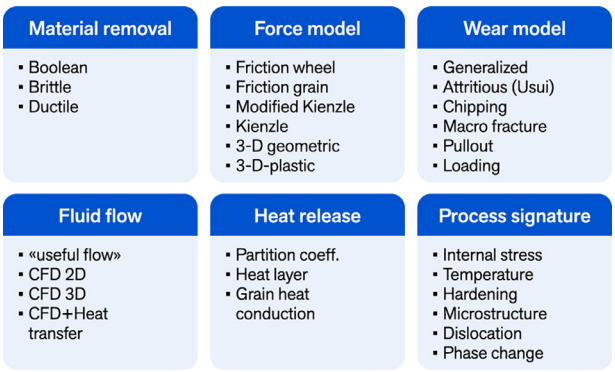


**Fig. 10.** Thermomechanical modeling modules.

### 3.2. Material behavior and the mechanics of abrasive processing

Material-removal mechanisms with fixed-abrasives typically fall into either (i) chip formation via plastic deformation in ductile materials or (ii) multiple crack generation (lateral and Hertzian) via brittle fracture in brittle materials [295]. Brittle materials can exhibit both brittle behavior and ductile behavior. Therefore, it is crucial to consider both. The material-removal mechanism in composite materials, such as Al-metal matrix composites reinforced by SiC particles, is understandably much more complex. It can involve a range of mechanisms, including refinement of Al grains (via dynamic recrystallization and dislocation) and stacking faults of SiC particles [120]. Accurate modeling of material removal requires models that describe a material's behavior under stress, strain, and temperature. Constitutive equations connect material parameters to material behavior under external loading. Any constitutive model in continuum mechanics can potentially be useful for simulating material removal. Models of many material types are readily available in commercial numerical-simulation software. However, their use requires knowledge of material parameters that can be obtained from standard material tests or machining experiments [249].

Please cite this article as: P. Krajnik et al., Advances in modeling of fixed-abrasive processes, CIRP Annals - Manufacturing Technology (2024), https://doi.org/10.1016/j.cirp.2024.05.001

*3.2.1. Ductile material removal*

Ductile constitutive equations require addressing aspects such as elastic behavior, hardening law, flow limit, flow rule, energy dissipation, recovery, damage, and failure. These aspects depend on temperature, which increases due to plastic deformation. Friction, stress, strain and chip formation during plastic flow – taking into account its dependence on temperature were modeled in [189]. This work emphasized the necessity of integrating material physics with the fundamental process mechanics. For a given material with a known yield shear stress and strain rate, the temperature in the plastic-deformation zone was derived, and the chip-formation was analyzed.

The Johnson-Cook (J-C) constitutive material model [145] is commonly used due to its simplicity and completeness. The hardening law defines isotropic hardening as a flow stress, which depends on strain, strain rate, and temperature. It accounts for the effects of strain hardening and thermal softening. The J-C model can also be extended to account for fracture by factoring in its dependence on strain. The extended model has been successfully applied to grinding, as demonstrated in [96,122]. Furthermore, a damage term can be included in the J-C model by defining a corresponding damage evolution equation. Formulating a failure model is thus possible, taking into account the gradual degradation and eventual failure of the material under loading conditions. All modules can be substituted, and in the case of the hardening law, either kinematic hardening or formative hardening can be employed [300]. However, the material behavior cannot be accurately described by isotropic hardening alone due to effects such as the Bauschinger effect. This is especially evident in cyclic loading. In the case of grinding, it results in deviating normal forces. Material models have been implemented in various environments such as FEM and smoothed-particle hydrodynamics (SPH). These models have been utilized to derive forces [101], temperature [6], chip shape [65], surface topography [260], residual stress [256], and burr [177,230].

*3.2.2. Brittle material removal*

The behavior of brittle material is more complex to model than ductile material. In brittle materials under specific conditions – such as high compressive stress – ductile behavior can be observed prior to the onset of brittle fracture. Various approaches have been adopted to describe this phenomenon. One approach includes incorporating isotropic hardening and damage evolution, as in the Johnson-Holmquist (JH-2) [146], Johnson-Holmquist-Beissel [147], and Simha [245] constitutive models for brittle materials. These approaches are often used to describe material behavior in ballistics tests [61]. Using similar strain rates, these models have also been applied to grinding processes [180,187]. The Drucker-Prager model [92], which considers an idealized material that behaves elastically until slip or yielding occurs, represents another useful approach. In some cases, the Drucker-Prager model has been extended to consider phase transformations. These modifications were employed to examine phase transformations that take place during loading [263] and cutting of silicon [262,265]. The bi-linear elastic yield curve accounts for crack-opening/displacement and shear modulus degradation. This approach has been implemented in contexts such as Vickers indentation [294] and single-grit scratching [51].

When grinding brittle materials, the workpiece strength has been shown to decrease due to subsurface cracking inherent in the brittle-fracture material-removal mechanism [282]. In addition, the scratch left by grit interaction cannot be described as Boolean removal of the projection surface, but is much larger due to chipping effects [175]. Lastly, the energy (and therefore heat) produced when grinding brittle materials is significantly lower compared to ductile materials: energy is proportional to the second power of the depth of cut for brittle removal and proportional to the third power for ductile removal [39].

Even for brittle materials, ductile cutting is possible under certain process conditions. The limit for the critical depth of indentation $d_c$ at which the ductile-to-brittle transition occurs is usually attributed to the Bifano [39] equation:

$$d_c = 0.15\left(\frac{E}{H}\right)\left(\frac{K_c}{H}\right)^2 \tag{12}$$

where $E$ is the modulus of elasticity, $H$ is the indentation hardness, and $K_c$ is the fracture toughness. The constant (0.15) applies except for materials in which $K_c$ varies significantly with indentation depth. This equation, although simple, provides a reasonable estimate of the ductile-to-brittle transition. However, its predictive accuracy is limited. Extensions that can enhance predictive accuracy include: (i) additional physical effects (such as dynamic viscosity, heat capacity, thermal conductivity and grinding-fluid enthalpy of vaporization), (ii) geometric parameters (rake angle and tool radius [82]), and (iii) phase transformations [265]. An extended ductile-to-brittle transition model was presented in [213]. A review of the mechanisms of ductile removal in brittle-material grinding indicates that while many experimental studies confirm the potential for ductile machining of brittle materials, the specifics are still being debated [134].

The primary challenges when modeling material behavior are (i) the accurate representation of the physical microstructural effects, and (ii) the reliable determination of the material-model parameters. Unfortunately, standard material testing cannot attain high-enough deformation rates in the shear zone to accurately mimic shear rates in grinding. Therefore, some researchers aim to identify the parameters directly from machining experiments [2,35,104,249]. While physically correct modeling of material removal involves the use of constitutive equations from continuum mechanics to describe plastic deformation and material separation, simplified analytical models utilize Kienzle-based equations for forces [15,244], scratch geometries as Boolean interaction [15,225,244,268], elastic springback, and analytical descriptions of burr formation (in ductile materials) [13,132], and shelling (in brittle materials) [217]. While parameter identification for modeling is generally performed using single-grit scratch tests, many studies use literature-reported parameter values for their constitutive models. These values can sometimes deviate significantly from the actual behavior of the work material due to batch variations and different heat treatments. For example, [49] used the JH-2 model to simulate ultrasonic-assisted grinding of silicon. This was done as a single-grit interaction with SPH, while the tool was assumed rigid and represented by an FEM mesh. However, thermal effects, crack growth or phase transformation were not considered. In contrast, [36] used a single-grit simulation utilizing a constitutive equation from [131]. The underlying material model to account for the high temperatures (exceeding 1300 °C) was obtained from the Split-Hopkinson Pressure Bar (SHPB) test. For silicon-carbide-fiber reinforced silicon-carbide (SiCf/SiC), the JH-2 material parameters were identified for SiC matrix and SiCf and configured within SPH simulation in LS-DYNA, providing predictions for the normal force in single-grit scratching of SiCf/SiC that closely aligned with empirical observations [178].

### 3.3. Grinding mechanics by field equations and numerical solutions

The workpiece surface is generated by a large number of geometrically undefined cutting edges. Thus, tangential and normal forces are calculated by summing the individual forces of all grit-workpiece interactions in the contact zone. Power and specific energy are computed by adding up power and energy expended in the grinding zone for all grit interactions. The stochastic behavior is accounted for using the Monte Carlo method, requiring many tool generations and subsequent numerical solutions. Given the extensive number of stochastic elementary tool-workpiece interactions, it is typically assumed that the behavior of all grinding wheels generated from one stochastic distribution is the same. However, this traces back the problem of solving the continuum-mechanics equations for different geometries of single grits. To synthesize the behavior of the grinding wheel, the solutions of the single-grit interaction are condensed into surrogate models to reduce the numerical effort required for simulating the

Please cite this article as: P. Krajnik et al., Advances in modeling of fixed-abrasive processes, CIRP Annals - Manufacturing Technology (2024), https://doi.org/10.1016/j.cirp.2024.05.001

grinding process. The basic assumption is that individual grits do not interfere with each other. All simulations, however, only compute a representative surface area and never the whole geometry. Single-grit interactions can be computed with FEM, SPH, DEM, and molecular dynamics (MD). While the latter suffers from small model sizes, FEM requires significant remeshing effort. A recent overview of simulation techniques, especially on DEM for brittle materials, is given in [143], including frequently used calibration and parameter identification techniques.

Simulating single-grit interactions is needed for accurate predictions of grinding results, particularly in the case of engineered grinding tools. The analysis of chip morphology is a fundamental approach that enables a better understanding of abrasive processes. This type of analysis offers insight into the underlying mechanisms (sliding, plowing, cutting) as well as their transitions. Several authors presented different strategies for understanding chip formation and its morphology. A MD model was proposed in [204] to analyze the nano-scale grinding of copper using diamond grits. In this work, the Morse potential function was used to simulate the process interactions. It was observed that increasing the depth of cut results in rougher machined surface and more frequent voids in the workpiece. Furthermore, utilizing a negative rake angle (−45°) generated compressive stress that caused the material to pile up in front of and underneath the grit. [53] developed a 2D FEM for ultrasonic-vibration-assisted grinding. This model considered the effects of ultrasonic vibration and infeed on chip formation, temperature, force, and stress. The results suggested that the hybrid process produced shorter, straighter chips and caused less plastic deformation of the ground surface, potentially improving the grindability of the tool steel. In [298], a 3D FEM model was developed to investigate the morphological evolution of grinding chips from a nickel-based superalloy using a single grit. The results indicated that as the cutting speed increased, the chips progressed from segmented to continuous. The chip segmentation frequency appears to be mainly determined by cutting depth and speed.

Meshless computational methods, such as SPH, which are not limited by deformation amounts, are a promising alternative for simulating chip formation and shape [230]. Further reinforcing this perspective, [159] presented a model that used a graphics processing unit, i.e. (GPU)-accelerated code with meshless methods to optimize diamond-wire sawing of silicon wafers. The goal was to reduce cutting loss and surface damage. The simulation results were compared to single-grit scratch experiments using real, non-idealized grit geometry. The J-C flow stress model was utilized to evaluate the applicability of the model to estimate the ductile-to-brittle transition zone. Fig. 11 shows an example: SPH simulation of material removal using the J-C model to describe material behavior. A friction model and local heat release have already been included. By applying the Corrective Smoothed Particle Method (CSPM) scheme to the SPH, chip curling could be simulated following the obtained experimental results [229,230].

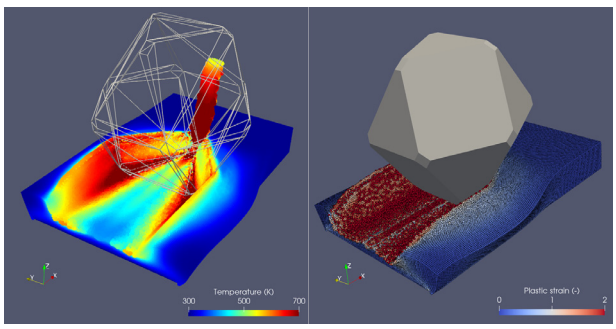


**Fig. 11.** Simulation of burr and chip formation with SPH solution on the GPU for a geometrically defined grit shape as hexa-octahedron [230].

A similar approach was used to model single-grit scratching and compare chip formation and shape for different diamond orientations, as shown in Fig. 12. The results indicate that diamond

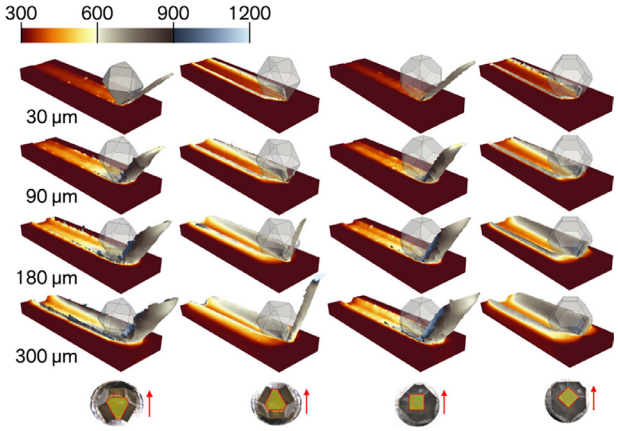


**Fig. 12.** Temperature distribution chip formation simulated with SPH at different penetration depths and grit orientations [98].

orientation affects chip-formation behavior and chip morphology, which underscores the suitability and efficiency of the SPH method for modeling single-grit scratching [98]. The capabilities of SPH were further demonstrated in [188], where the debris size of the removed material was computed for bone cutting, along with the material separation based on both stress and strain criteria.

### 3.4. Synthetization of grinding wheels from single grits

Different grit orientations result in different chip shapes, surface traces and burrs. This must be taken into account when simulating the interaction between a grinding wheel and a workpiece. Considerable wear effects can be expected when subsequent grit paths overlap, as the trailing grits come into contact with the work material and burrs from the previous grit paths. To reduce computational time, a GPU can be used for parallel computing to simulate a complete grinding wheel with numerous grits in contact. Fig. 13 illustrates the stochastic distribution of grits on the grinding wheel interacting in sequence with the workpiece material, which has been altered by the previous grits.

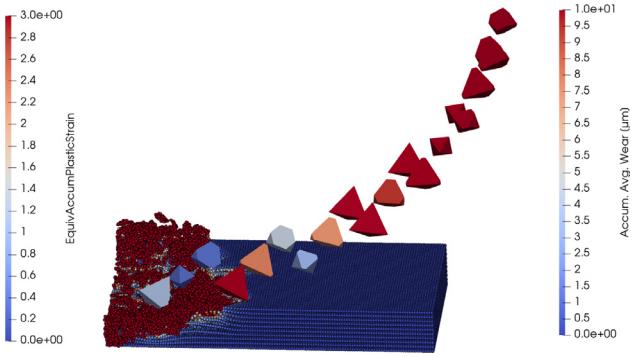


**Fig. 13.** GPU-based SPH simulation showing the parallelization capabilities of GPU [229].

The synthetization of the grinding wheel, comprising geometrically simplified grits for the simulation of material removal with SPH in LS-DYNA, was presented in [297]. The approach is shown in Fig. 14. This application refers to the dynamic tool behavior for plaque removal in rotational atherectomy. The interaction between different grits occurs through overlapping grooves. The calculated grinding forces were in good agreement with experimental results after identifying J-C material parameters.

Single-grit scratch tests with overlap between leading and trailing grits were conducted by [58]. This work, however, did not specify the hardening law. Therefore, the model predicted the influence of the

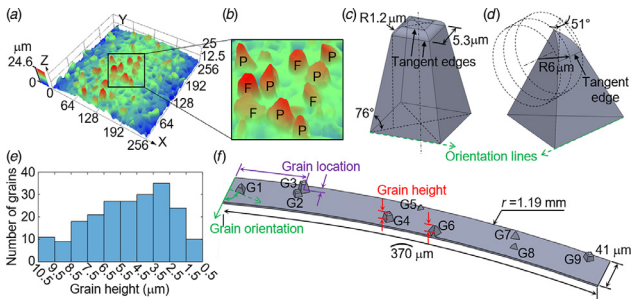


**Fig. 14.** Synthetization of a grinding wheel from stochastic placement and orientation of grits [297].

preceding grit only by the change in workpiece surface topography. [66] investigated the interaction between two subsequent grits for the grinding of SiC. The overlap of von Mises stress fields of the two grits was seen as the reason for an increase in tangential forces, although no hardening law was specified. On the other hand [80] included phase transformations between ferrite, austenite and martensite according to the transformation law [110] which included phase transformations induced by plastic strains. By considering the phase change, it was possible to calculate the residual stress field (Fig. 15) and select process parameters to reduce tensile residual stresses.

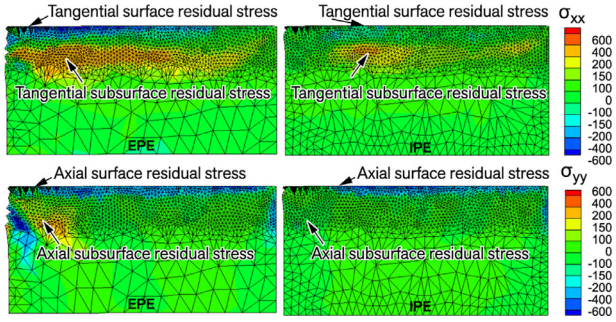


**Fig. 15.** Residual stresses in tangential (XX) and lateral (YY) direction. EPE excluding phase transformation, IPE including phase transformation [80].

The interference between two grits scratching simultaneously in close proximity to each other in brittle-hard materials (such as SiC) was studied using a Johnson-Holmquist approach for the constitutive equations (damage and failure model) by [93]. When the process zones of two different grits are in proximity, the crack systems interfere. This creates a larger damage zone than what is observed from two single-grit scratches, as shown in Fig. 16. Here, a coupled FEM-SPH model was employed – where SPH was used in the areas where material removal occurs, and FEM was used in the areas below the material removal.

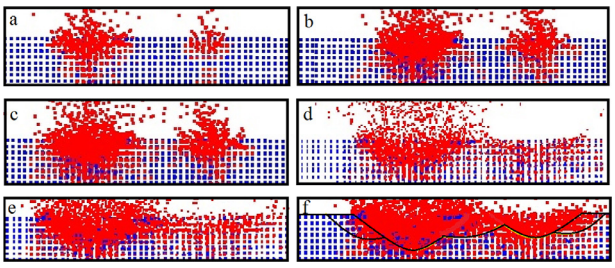


**Fig. 16.** Overlap of damage fields (highlighted in red) and cracks during a double-scratch scenario, as illustrated in SPH simulation [93].

By using FEM and the J-C constitutive model, [96] showed how subsurface damage changes with increasing cutting-edge radius. [114] developed a single-grit scratch model using the J-C approach to study the cutting of SiC-particle reinforced aluminum alloy. Bonding behavior was identified through a SHPB testing. Additionally, [142] examined the interaction between a DEM represented workpiece and a grinding wheel composed of equally-shaped, evenly-spaced grits, while [185] analyzed exit burr with a J-C constitutive equation that incorporated damage.

### 3.5. Grinding forces

As discussed in Section 2.1, the fundamental parameter that characterizes the efficiency of material removal is the specific energy (Eq. (1)). Therefore, process mechanics must account for this parameter. The specific energy is directly related to the tangential force, and it is well established that the total force is comprised of the sum of the forces of the three component grit-workpiece interactions: sliding, plowing, and chip formation (cutting) [202].

Macerol et al. [191] recently introduced new wheel-workpiece interface laws based on the established Malkin and Cook models for the cutting and sliding force components [199]. Instead of power derivations, a first-principles approach was used to obtain the stress relationships in the abrasive contact. By accounting for the effects of process geometry and kinematics via the use of the aggressiveness number (from Eq. (5)), the effect of different grit types and dressing conditions on grinding-wheel topography was evaluated. For example, the effects of grit protrusion and wear-flat area were correlated to parameters such as (i) the intrinsic specific grinding energy, (ii) the sliding component of tangential stress, (iii) the force ratio, and (iv) the friction coefficient. This work showed that by considering the above parameters, it was possible to accurately quantify the influence of grit properties and dressing conditions on the performance of the grinding wheel.

The Kienzle model [157,158], applied to a range of processes including grinding [47,112,169,244], can be expressed as:

$$F_c = k_{c1.1} \cdot b_D \cdot {h_D}^{1-m_c};\ F_c = k_c \cdot {A_{ch}}^{1-m} \tag{13}$$

where $F_c$ represents the cutting force. The factor $k_{c1.1}$ is the unit specific cutting force, $b_D$ the undeformed chip width, $h_D$ the undeformed chip thickness, and $m_c$ is a work material-dependent parameter that needs to be determined experimentally. The specific cutting force is denoted by $k_c$, whereas $A_{ch}$ is the cross-sectional chip area. In grinding, the exponent $m$ is often set to 0.

The utilization of the Kienzle equation provides a "surrogate" model where the interaction of individual grits with the work material is simplified to the removal of the interference volume. This implies that the grits are reduced to their projection area in the cutting speed direction, as shown in Fig. 17.

A recent review [207] discussed the advances and methodologies in grinding-force modeling over the past 15–25 years. Models were categorized into macro and micro types.

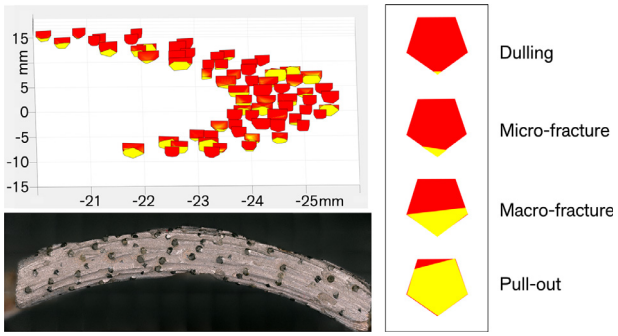


**Fig. 17.** Simplified two-dimensional depiction of grits for modeling a complete grinding wheel in face grinding [10].

### 3.6. Wear modeling

Wheel wear is an inevitable phenomenon in grinding. It results in size and form errors in the workpiece and increased forces (and heat) due to grit dulling. As a result, the workpiece quality suffers. Fig. 18 provides an illustration of the various wear phenomena.

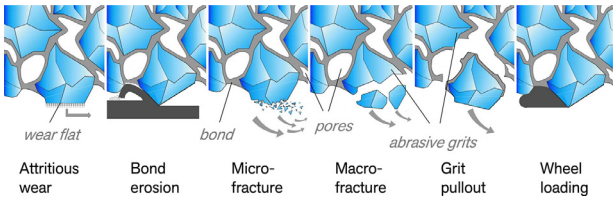


**Fig. 18.** Wear phenomena in grinding wheels (adapted from [108]).

Wheel wear predominantly manifests in two forms: attritious wear and fracture wear, each with distinct mechanisms and consequences, as shown by Malkin [199,200]. Attritious wear – also called flattening and dulling – arises from high mechanical-thermal loading and chemical interactions between the abrasive grit and workpiece. This type of wear typically increases the grinding forces, which can lead to grit fracture and bond fracture (grit pullout). Grit fracture wear entails the loss of abrasive material as fragments break from the grit, either on a micro scale or a macro scale. Such fracture occurs when the induced stresses on the grit exceed its rupture strength [109]. When a bond fails, the grits are pulled out from the grinding wheel. In addition, the bond is subjected to erosion and abrasion. This reduces the grit-retention strength, which can result in premature grit pullout [182]. The bond strength and grit strength influence the likelihood of fracture, with the weaker of the two precipitating the loss. The primary determinants for a grit pullout are the shear stresses at the grit-bond material interface and the interfacial strength of the bond along with the associated retention forces [47]. Loading of the intergranular space – i.e., the pores – increases friction and normal forces, thereby limiting the material removal by the grits, which can be considered a wear phenomenon as well. Therefore, any model attempting to describe wear must consider these series of actions, particularly emphasizing the increasing forces due to dulling as the main catalyst for other wear mechanisms.

Most wear investigations are experimental. For example, to optimize the wheel specification and consider wheels with different specifications along the profile, research has been carried out to investigate the effects of cBN grit shape [192], grit concentration and grit toughness on grinding performance. Abrasive grits with higher aspect ratios (elongated grits) exhibit higher wear rates and vice-versa. Tougher grits generally exhibit lower wear rates, but only if they are combined with an appropriate bond [190,191]. Nevertheless, wear investigations can also combine experiments with theory, including modeling. A study on the impact of wheel wear on the grinding performance of electroplated cBN wheels was conducted by [119]. An analytical model was used and power was measured to predict wheel wear-flat area for wheels at different states of wear. A similar study [132] aimed to explore the correlation between grinding specific energy and wear. The findings indicated that variations in specific energy correlate with wear-flat area. Another theoretical study analyzed the number of active cutting edges and the grit-workpiece interference area on the wheel-profile wear [50]. The cutting-point spacing between grits as measure for pullouts was determined through SEM observation, while the height distribution of cutting-edge protrusions was measured with 3D confocal microscopy.

In grinding of cemented carbide and, in particular, superhard materials (PcBN and PCD) for cutting inserts, the diamond wheels are subjected to severe wear. Unfortunately, modeling of wear in insert grinding is limited. Denkena et al. [72] modeled the wheel and workpiece geometry, kinematics, and oscillation. In the kinematic simulation, the path of the contact point was first calculated. This resulted in multiple path overlaps. Subsequently, the contact area along the calculated path was represented by progressively smaller elements until sufficient convergence was achieved. The simulation outputs included the accumulated number of grit engagements and the proportion of the area with the same number of grit engagements in the total grinding layer area. The distribution of the predicted G ratios was determined from these calculated area proportions. The assumed wear mechanisms were grit micro fracture and grit pullout.

Wear investigations using model-based methods often focus on considering several mechanisms within the modeling parameters to determine the dominant wear mechanism – while avoiding excessive complexity and computational effort. Models for attritious wear are generally adopted from metal cutting. These consider parameters such as contact stress, relative sliding speed, and temperature. Temperature has a significant effect on activation energy, especially for diffusion processes. One approach to account for the wear of abrasives is to simulate the recession of the surface of the individual grits during grinding, as in case with geometrically defined cutting edges. Usui's model [259] can be used to predict the wear rate due to normal stress, sliding speed, and temperature, based on:

$$\frac{dW}{dt} = A_1 \sigma_n v_{sl} \exp\left(-\frac{A_2}{T}\right) \tag{14}$$

where $W$ is the depth of wear, $\sigma_n$ is the normal stress on the contact surface, $v_{sl}$ is the sliding speed, and $T$ is the absolute thermodynamic temperature, with $A_1$ and $A_2$ being constants. The determination of these constants requires a significant number of experiments for different tool-work material combinations. Therefore, attempts have been made to develop physics-based models utilizing thermodynamic calculations with reduced experimental effort [198]. Physics-based models, however, are not widely used. Instead, simpler methods integrating Usui's model into FEM simulations are preferred. As an example, a 2D-FEM simulation [286], utilizing Usui's model, was developed where the individual nodes of the tool mesh were moved along the inward normal to the tool surface by the calculated wear rate at each time step. Another approach combined temperatures obtained from a 3D-FEM with the modified Usui's model, which resulted in an improved model for wear prediction [196]. However, such approaches are likely overly complex when applied from a cutting insert to a large number of grits. Therefore, the wear models should be applied in a more generalized manner, where forces (instead of normal stress) are simulated, sliding speed is derived from the process kinematics, and temperature is derived from a simplified energy model [169,170], which can describe dulling and force increase, as well as the modification of the grit geometry.

Malkin [243] established that fracture is the main factor in the wear of a single grit. In a related study, [287] used an FEM simulation to model the fracture of a single cBN grit, integrating the J-C model [145] to simulate chip formation. Brittle fracture in cBN was found to be primarily caused by the maximum tensile stress [139,140]. The detection of crack initiation was accomplished using the Rankine criterion, which detects when the maximum principal tensile stress surpasses the tensile strength of the brittle material. In this case, simplifying assumptions were made regarding the stress distribution in the grit. During the simulation, the grit's geometry was updated by removing the failed elements and adjusting the boundary nodes in accordance with the shape modification. Two studies [109,140] found that compressive failure occurs at the tip of the grit, in addition to tensile failure. This compressive failure was integrated into FEM simulation [264] that can simulate different phenomena, such as the propagation of cracks, volume loss resulting from macro fractures, and micro-fractures near the abrasive tip [287].

The wear behavior of a grit modeled using DEM [105] proved more suitable than FEM due to the simplicity of detaching

discrete elements and DEM's capability of retaining a third body after the detachment of elements. The grit was discretized using spherical discrete elements, while the material behavior was simulated via a 3D cohesive beam model connecting discrete elements. The failure criterion was established as the Von Mises stress exceeding the micro-fracture failure stress assigned to the beams. The wear occurred when the discrete elements detached from the primary body. In [222], simulation of volumetric wear of vitrified grinding wheels was performed, also with a multiscale model, by integrating the mechanical behavior of bonds and the stochastic nature of grit positions in a wheel. Here, a DEM microscale model and its randomization could be used to simulate the stress field in the contact zone and predict the volumetric wear by accounting for the detachment of grit-element clusters from the bond.

Simulation of wear can be also approached via kinematic-geometric modeling. A simulation model was developed in [225] that combined tool, material removal, and wear models. The dominant wear mechanism was micro-fracture of grits. The 3D grit geometry was simplified, with micro-fracture modeled as alteration to the profile orthogonal to the cutting speed. [217] modeled diamond-wire sawing, employing a similar approach of projecting 3D grit meshes along the cutting direction (Fig. 19).

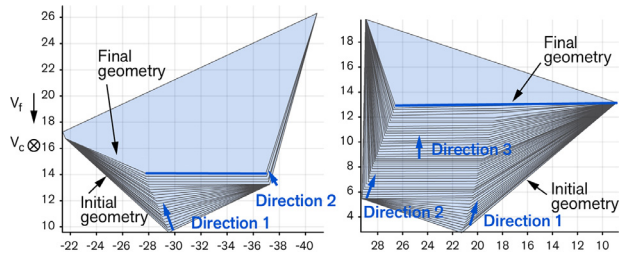


**Fig. 19.** Alteration of 2D grit geometries with progressing wear [217].

Abrasive wear was calculated via the Usui model [259], and grit vertices were shifted at every time step to propagate wear. The model showed its ability to create dull grits or new grit edges. Grit pullouts were modeled with a moment balance for the grit under the effect of grinding and retention forces. The bond wear progressed through a reduction in bonding height, increasing the stress in the bond. To simulate such wear progression, [276] used a stochastic method, generating an experimentally obtained database of grits at different wear states. This wear-dependent stochastic grit model was used to simulate grinding wheels with arbitrary grit shapes and could predict surface topography and grinding forces at various states of wear.

Another study [23] used large-scale MD modeling due to its capacity for mesh-free simulations, which are especially useful in cases of large deformations and significant material loss. However, their approach was restricted to the sub-micrometer range, implying a need for upscaling. [299] examined the wear of a crystalline substrate caused by an abrasive particle on a nanoscale level. The results indicate that the amount of wear is proportional to the sliding distance, which is in line with Archard's law [11]:

$$W = A_3 \sigma_n L_{sl} H^{-1} \tag{15}$$

where $L_{sl}$ is the sliding distance and $H$ the hardness. In [95], MD was used to simulate the abrasion process of a metallic surface by abrasives. By observing the wear depth over time, it was demonstrated that Barwell's macroscopic wear model [30] is applicable at the atomic scale. The wear depth $W$ was described by a model that combines Barwell's wear, represented by an exponential decay term characterized by the time constant $\tau_w$, with a steady-state wear contribution $W_c t$:

$$W(t) = W_0 \tau_w \left[1 - \exp\left(-\frac{t}{\tau_w}\right)\right] + W_c t \tag{16}$$

where $W_0$ is the initial wear (depth) at time $t = 0$.

Concerning wheel loading/clogging, different models were proposed. For example, the volume of the loaded work material was analytically modeled considering temperature-dependent workpiece hardness, adhesion coefficient, and process geometry and kinematics [1]. A similar model analyzed asperity yielding and adhesive wear, accounting for metal transfer due to work-material adhesion on grits, stress-induced crack initiation and propagation, and grit-workpiece contact deflection [3].

### 3.7. Modeling of fluid flow and temperatures in grinding

Grinding operations usually use a grinding fluid for cooling and lubrication. The 2020 CIRP keynote by Heinzel et al. [130] addressed fluid flow and dynamics, heat transfer, and chemical interactions between grinding tools and fluids. It also gave valuable empirical results. The modeling mostly focused on nozzle design, which will be omitted in this discussion.

Modeling of fluid dynamics in grinding can involve analyzing the fluid flow within the grinding zone to determine the hydrodynamic forces. A typical modeling approach includes computational fluid dynamics (CFD), which enables the development of multivariable and multiphase models. Flow rates, hydrodynamic pressure, heat transfer and temperatures in the contact zone are predicted with 2D-CFD and 3D-CFD simulations. CFD analysis can provide valuable insights into the interaction between the fluid and the grinding wheel and workpiece, as well as its effects on the temperature field. When fluid flow mainly occurs in one plane, 2D CFD models are often used [209]. The FEM and Finite Volume Method (FVM) are numerical tools that are utilized in CFD to approximate solutions to the partial differential equations that describe fluid flow. These methods differ in their approach to spatial discretization and derivation of the underlying algebraic equations. FVM is a more widely used method, preferred for its conservational properties and greater ease of programming compared to FEM. These models are simpler and faster to run than their 3D counterparts. However, they may not fully capture the complexities of the flow.

For example, the utility of 2D-CFD simulation is limited because of the centrifugal forces acting on a rotating grinding wheel. As a result, several researchers have used 3D-CFD models to investigate the interactions between the wheel and fluid, such as fluid velocity, pressures and nozzle designs [130]. 3D-CFD models are mainly used for the purpose of visualizing and optimizing internal nozzle flow. Recent CFD applications have used the Shear Stress Transport (SST) k-$\omega$ model, a useful turbulence model capable of handling various turbulence scales as demonstrated in [31,248]. 3D fluid flow in cylindrical grinding was simulated by incorporating not only the fluid, but also the large surrounding environment and the grinding gap [31]. This shows several challenges: the simulation must consider both gas and fluid phases and handle significantly different levels of discretization. Fig. 20 depicts the velocity vectors in three-dimensional fluid

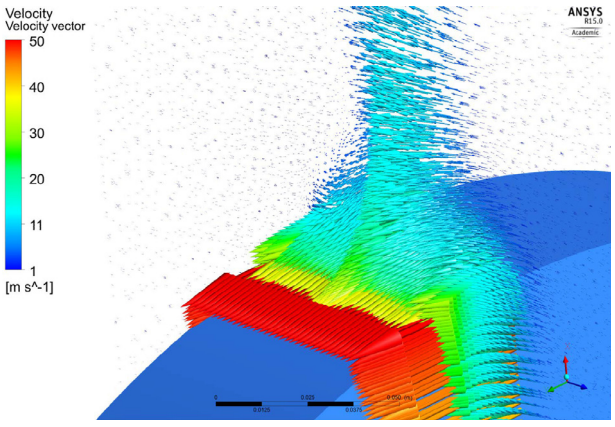


**Fig. 20.** Visualization of air flow around the grinding wheel [31].

flow caused by the grinding wheel's "pumping" effect, influenced by centrifugal forces that affect drag flow [31].

During grinding, most of the generated power is converted into heat. A fraction of that heat enters the workpiece, which can lead to thermal damage, or "grinding burn", which is characterized by tempering, residual tensile stresses, or phase changes in the microstructure [201]. Heat-transfer models require assumptions about the energy partition, i.e., the fraction of heat entering the workpiece. They then calculate the resulting temperature distribution within the workpiece. Most analytical models that calculate the workpiece surface temperature are derived from the classical Jaeger's moving heat-source theory [141], which approximates the grinding zone as a band heat source moving along the workpiece surface at the workpiece velocity. [233] provided a fundamental unified approach to model temperatures in high efficiency deep grinding (HEDG). This work demonstrated strong experimental evidence for very high fluid convection cooling in low temperature grinding. Thermal analysis of grinding was reviewed in the 2007 CIRP keynote by Malkin and Guo [201]. The analytical models presented in this landmark work continue to represent the state-of-the-art.

Because of grinding's dynamic nature, the accurate determination and validation of a heat-transfer coefficient poses a significant challenge [130]. Additionally, the heat-dissipation ratios into the workpiece, chips, wheel/grits, and grinding fluid remains speculative. To overcome this, it is necessary to employ indirect methods. These typically involve correlating the outcomes of thermal and thermofluidic models with temperature measurements in the workpiece and/or grinding wheels. This critical step ensures the validation and accuracy of thermal modeling. Recently published simulations were validated using thermocouples embedded in a workpiece [168] and an infrared camera [135] to compare the predicted and measured temperatures. Drazumeric et al. [87] provided an alternative method by modeling the workpiece temperature as a function of position along the contact length and depth beneath the surface. Comparisons were made between the work material's rehardening temperature and the depth of the rehardened layer measured in the workpiece, enabling the reverse calculation of the grinding temperature at the surface. However, this required a certain experimental effort, as several workpieces had to be ground to deliberately induce workpiece rehardening.

To improve the accuracy of the thermal simulations, it is important to include the influence of grinding fluid on heat partition and temperature. The heat-transfer coefficient, influenced by properties like specific heat capacity, thermal conductivity, density, and viscosity, characterizes how heat is exchanged between the workpiece, grinding wheel, and grinding fluid. A recent study on the fluid convection models [293] also reviewed advances in convection modeling. By inputting values for these properties, CFD simulations enable a more accurate numerical analysis of heat transfer in grinding.

### 3.8. Process signatures

The concept of process signatures [46,152] is an approach for predicting work-material alterations. It characterizes fixed-abrasive processes based on the energy they convert and dissipate within the work material, based on the process parameters and generation dynamics. This concept enables the evaluation of variations in properties such as hardness, residual stress, microstructure, and chemical composition. It achieves this by correlating internal material loads, such as stress, strain, and temperature, with the resulting alterations. For example, the prediction of residual stress at the workpiece's surface subjected to thermal load was reported in [172]. Using 2D-FEM simulation, it was possible to establish a correlation between the surface tangential residual stress and the maximum surface temperature. This was achieved by assigning a heat partition to the workpiece and then calculating the maximum surface temperature and temperature gradient by integrating the time-dependent heat flux into the workpiece. In a similar manner, FEM simulations were used to determine the stresses and strains in the workpiece [100]. In a recent study, FEM and experimental temperature-time histories were used to evaluate grinding-induced thermal loads at the workpiece surface and subsurface [160]. The study found a correlation between variations in hardness and the temperature-change rate at given peak temperatures. It also unveiled the connection between hardness change and the Hollomon-Jaffe parameter, which considers both the absolute temperature and its time evolution. Additionally, the study demonstrated that when there was no significant tempering of the workpiece, there was a correlation between surface residual stresses and the maximum local temperature gradients at the surface.

### 3.9. Process-machine interactions

Grinding is often the final step in the production chain [128,165], so even small influences from a machine can play a significant role on the quality of ground components. Several papers gave an overview of process-machine interactions [14,42,73]. Models that consider the grinding machine typically include both a process model (as already described) and a machine model, with the grinding wheel typically considered as one component of the machine or as a third component. The models can be combined into a single set of time-differential equations or solved in a staggered manner – i.e., solving the machine model first and then the process model. Another method involves an iterative process where solutions from both the machine and process models are used to update each other at each time step [15]. The coupling of equations is done via the process forces acting on the machine, with machine displacements being fed back into the process model. Both models are typically simplified. The machine can be simplified to a one-mass model or a rigid body model. Its relative motion can be represented by the first few eigenmodes, or the frequency response functions for the tool center point [43]. The main objectives of analyzing process-machine interaction are the avoidance and analysis of instability, the prediction of surface quality, and the assurance of workpiece accuracy, especially in gear grinding. A simplified rigid-body model for pendulum and speed-stroke grinding was presented in [272]. Biermann et al. [37] investigated process-machine interaction in free-form grinding using a dexel model to depict the wheel-workpiece contact behavior as a discretized representation of functions defined on surfaces. A removal predictor calculates process forces, and the iteration stops when the cutting forces and the contact forces coincide. The wheel rotation was taken into consideration via an arbitrary Euler-Lagrange model. A similar 3D dexel model was applied to tool grinding [70] to consider the effect of fluctuating stiffness during the process for an accurate representation of the workpiece dynamics. [99] utilized a more sophisticated grinding wheel and process model which included single hexahedron-shaped grits distributed stochastically on the wheel surface, whereas the wheel body and the spindle shaft were modeled by FEM. In [69], the grinding wheel surface was modeled by superposing eccentricity, waviness, and roughness elements.

For continuous-generating gear grinding, a non-linear model was developed in [77]. The cutting and normal forces were found to be proportional to the interaction surface at all wheel-workpiece contact points. The machine's behavior was modeled with the eigenmodes of a rigid body model. Fig. 21 shows a simulation result depicting the flank and profile form deviation of the gear teeth; the results aligned well with the measured deviations.

In centerless grinding, the achievable roundness depends on the interaction between the machine and the workpiece. This was shown already in 1965, when studies were conducted on the work-regenerative waviness depending on the dynamic characteristics of the machine [232,234]. A similar approach combined previously separate modeling of workpiece dynamics and the geometric mechanism of the rounding process [164]. The analytical process models were also

Please cite this article as: P. Krajnik et al., Advances in modeling of fixed-abrasive processes, CIRP Annals - Manufacturing Technology (2024), https://doi.org/10.1016/j.cirp.2024.05.001

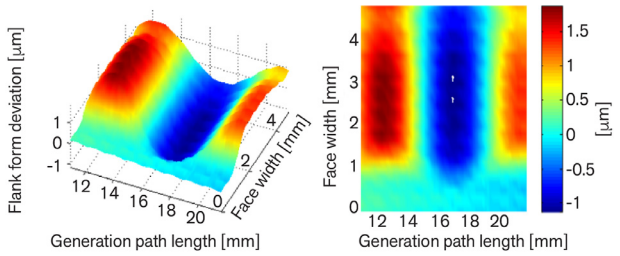


**Fig. 21.** Flank form deviation simulated with a coupled process-machine model for continuous generating gear grinding (adapted from [78]).

extended from 2D (plunge) to 3D (throughfeed) applications in [90]. Stability charts for both plunge [26] and throughfeed centerless grinding [125] can be used to avoid critical parameters that cause roundness errors. In addition, understanding process-machine interaction is required, for example when using active dampers, shown in Fig. 22.

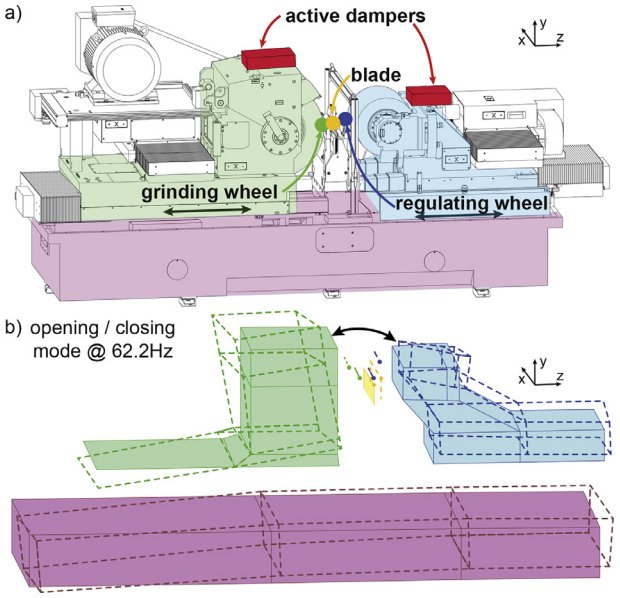


**Fig. 22.** Centerless grinder equipped with active dampers (a). Critical mode responsible for chatter vibrations (b) [28].

## 4. Modeling – data driven

In the era of digitalization, the importance of data-driven models for abrasive processes is becoming increasingly recognized for two reasons. First is the progressive advancement of grinding machines now equipped with external sensors. This provides high-frequency readings from both machine controls and sensors [278]. Second, data-driven models demonstrate advantages in areas where physical and simple empirical models tend to exhibit weaknesses. In contrast to physical models, less fundamental process understanding is required to make decisions based on measured process results, for example surface roughness. Some advantages over FE and MD models are the lower startup and computational efforts [44]. Given the increasing availability of grinding data and the potential for real-time application in manufacturing, data-driven models provide new opportunities for process control. These models can be particularly effective for industrial applications, offering insights into both the workpiece and the tool [71]. Note that data-driven modeling is closely related to AI/ML – where ML is a subset of AI focused on learning from data and making predictions based on data input. Interestingly, the "*Application of Artificial Intelligence in Grinding*" was addressed in a CIRP keynote already 30 years ago, back in 1994 [236].

In the context of this paper, data-driven modeling refers to the utilization of time-series data from external sensors or internal machine controls as inputs for ML models to estimate grinding results and make process adjustments. Therefore, data-driven modeling is concerned with ML approaches that allow to extract knowledge from data and learn from it autonomously. Since 2006, ML models have seen rapid advancement and have gained considerable scientific relevance. This trend is evidenced by a significant increase in literature found with Scopus when searching for "Machine Learning in Grinding" (see Fig. 23).

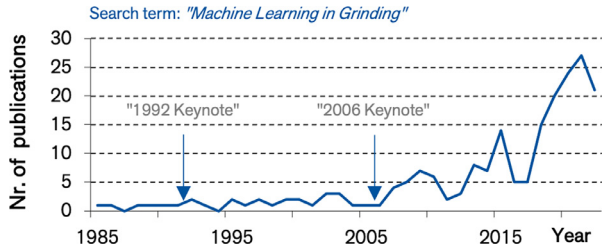


**Fig. 23.** Scopus entries related to "*Machine Learning in Grinding*".

A data-driven model is developed in five steps (see Fig. 24):

1. Acquisition of raw signals from sensors and machine control
2. Pre-processing of the raw signals
3. Feature extraction
4. Feature selection
5. Model construction

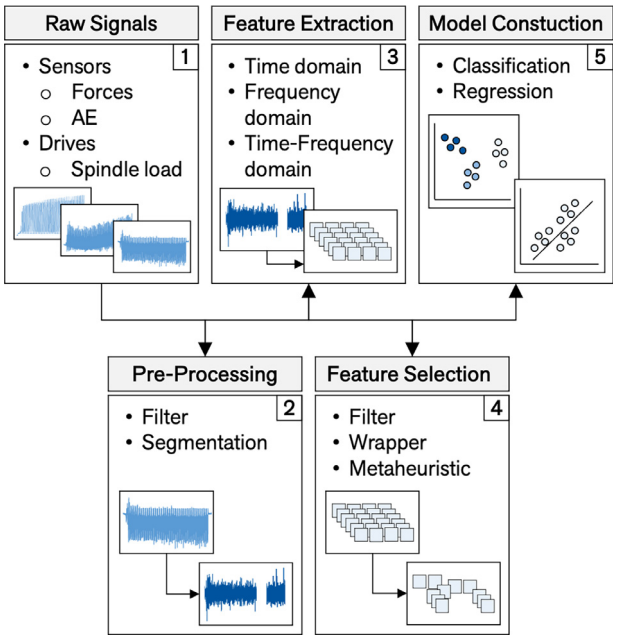


**Fig. 24.** Procedure of data-driven modeling.

The *raw signals* are acquired by the data acquisition (DAQ) and storage architecture of the machine tools. This architecture includes both hardware (for reading the raw signals of the external sensors and the machine controller) and software (for processing these signals). The raw data is stored near the machine, on dedicated databases, or in the cloud [154]. The raw signals mainly originate from temperature, optical, force, acceleration and/or acoustic-emission (AE) sensors. The power or current from the spindle and axes drives are also recorded [221]. Sensor selection depends on the output required by the model and the available processing and memory

resources. AE is very useful for collision detection and for mapping the process. However, AE requires a high sampling rate – in the MHz range – which requires both a suitable DAQ and high memory capacities. Acceleration sensors have the second highest sampling-rate demands, followed by force sensors and machine-internal drives [84].

During the *pre-processing* stage, the raw signals acquired from the sensors, or the machine controls are segmented and filtered in order to eliminate or minimize interference noise, divide the signals into individual events, or exclude idling.

Except for optical sensors, raw data (e.g., force or AE) are recorded as time-continuous signals (i.e., magnitude vs. time). *Feature extraction* transforms the continuous time series data into discrete data for use as model input. This process involves determining so-called "features" from the time-series data using mathematical calculations such as Fourier transforms. Feature extraction can be performed either by (i) specific selection followed by manual application of the calculations, or (ii) the automated use of programs such as TSFEL [24,63]. Feature extraction in the time domain uses calculations such as the root mean square (RMS), variance, skewness, or kurtosis of the raw signal. A major advantage is the fast calculation speed of features directly from the time domain. A potential disadvantage is the influence of interfering signals if careful signal pre-processing is neglected. Nevertheless, feature extraction in the frequency domain is mostly performed after executing a fast Fourier transform (FFT) on the raw signal. Unlike feature extraction in the time domain, features in the frequency domain can be selectively considered or excluded. However, due to the absence of temporal resolution, feature extraction in the frequency domain is only suitable for stationary processes. Techniques such as short-time Fourier transform (STFT) or discrete wavelet decomposition (DWD) provide a time and frequency-dependent feature extraction by transforming the raw signal into the time-frequency domain.

A subset of the extracted features is selected for model construction. This is called *feature selection* and demands a high computational effort [194]. This feature-selection process should (i) avoid collinearity in the model input data or overfitting during model construction, and should (ii) reduce computation time. Different feature-selection procedures are available, including filter-, wrapper or metaheuristic methods [83].

The last step is *model construction*. After the feature selection process, the remaining features serve as input data for ML models. Previous research in abrasive processes has predominantly focused on constructing supervised ML models. Here, an ML algorithm is provided with both input data and corresponding results/outputs. During the training phase, correlations and dependencies between the input and output data are determined and a statistical (empirical) "black box" model is formed. Then, during the validation phase, the trained ML algorithm is applied to unknown data. Models are typically differentiated into regression models, which estimate continuous results/outputs, and classification models, which predict discrete results/outputs [8]. For abrasive processes, most classification models are used to determine grinding-wheel wear or to identify thermal damage in the workpiece.

In this section, an overview is given of the state-of-the-art, data-driven models for wheel-wear prediction, surface-roughness prediction, grinding-burn detection and process diagnostics. The focus is on the type of sensor data required for the respective outputs and how the subsequent time series analysis – including feature extraction, feature selection and model construction – should be designed. Features can also stem from auto- and cross correlations, entering into sensor fusion, as seen when folding one sensor signal with the time series of another signal. Model evaluation often relies on statistical parameters such as the correct classification rate (for classification models) or the coefficient of determination (for regression models). These parameters are influenced by factors such as data quantity/quality or model task (e.g., the number of classification states).

### 4.1. Data-driven wheel-wear prediction

The performance of grinding wheels is significantly impacted by wear as discussed in Section 3.6. As macro-wear of the grinding wheel progresses, the dimensional accuracy of the workpiece decreases. Meanwhile, as micro-wear of the grinding wheel progresses – i.e., dulling of the grits – grinding heat increases (increasing the risk of thermal damage) and normal force increases (leading to a decrease in workpiece dimensional accuracy and an increase in the risk of vibration-induced surface distortion) [59]. Monitoring both macro and micro wear, coupled with data-driven models, offers the potential to increase workpiece quality, reduce costs, and reduce workpiece scrap. In addition, dressing intervals can be adjusted and optimized based on measurements and modeling of grinding-wheel wear, reducing wheel consumption.

Data-driven models for wear prediction primarily consist of supervised ML models for classification. The grinding-wheel wear is commonly defined as a result variable by two or three wear states, which are derived either by evaluating the grinding wheel volume loss as a function of the ground workpiece volume or by the change in workpiece roughness. In the classification of the wear states, published works mainly differ in whether the features for model input are extracted from the time, frequency, or time-frequency domain. AE sensors serve as the main signal source.

In surface grinding, discrete hidden Markov models for prediction of the wheel wear states were developed. The RMS signal from an AE sensor was the input for the model [237]. Another study used a decision-tree algorithm for classification [211]. Both studies considered only a few features from the time domain as model inputs, and a manual approach was employed for feature selection. The feature-extraction approach was further extended by transforming the acquired AE signal into the time-frequency domain via discrete wavelet decomposition and forming an autoregressive model [269]. Here the energy of the wavelet components and the model coefficients of the autoregression model served as features. As a feature selection method, an ant-colony optimization was developed. The discrete wavelet decomposition approach was further developed by initially filtering the raw signal with a 90-kHz cut-off high-pass filter [283]. Compared to direct decomposition of the raw signal, filtering resulted in better model quality. The RMS value and variance of the decomposition coefficients were calculated as features. Classification was executed by a Support Vector Machine (SVM) without prior feature selection. This wavelet-analysis approach was continued, but instead of the SVM, the C4.5 decision-tree algorithm was used [75]. In contrast to the previous approaches, a model for the detection of a worn grinding wheel was developed based on evaluations of sound signals using a microphone [176]. As opposed to using an AE sensor, which requires high sampling rates, a microphone can be sampled at lower sampling rates of 44.1 kHz. The raw signal of the recorded grinding passes was then transformed into the frequency domain via an FFT. The individual frequency spectra between 300 and 500 Hz were used as features. Then a Convolutional Neural Network (CNN) was applied to classify the grinding wheel wear.

The procedure for predicting wheel wear in cylindrical grinding was similar, using acceleration and AE signals. A comparative study analyzed decision tree, ANN and SVM models for the classification of two wear states based on four extracted time-domain features [12]. An AE sensor attached to the tailstock served as the signal source. The SVM classification model delivered the best results. In contrast, another study used an accelerometer instead of an AE sensor and computed features for the SVM-classification model using a time-frequency extraction based on a Hilbert-Huang transform [194]. This vibration-monitoring approach, using a 10 kHz sampling rate, presented a relatively cost-effective alternative to AE sensors for wear detection, particularly considering the amount of data required. The use of Hilbert-Huang transform

Please cite this article as: P. Krajnik et al., Advances in modeling of fixed-abrasive processes, CIRP Annals - Manufacturing Technology (2024), https://doi.org/10.1016/j.cirp.2024.05.001

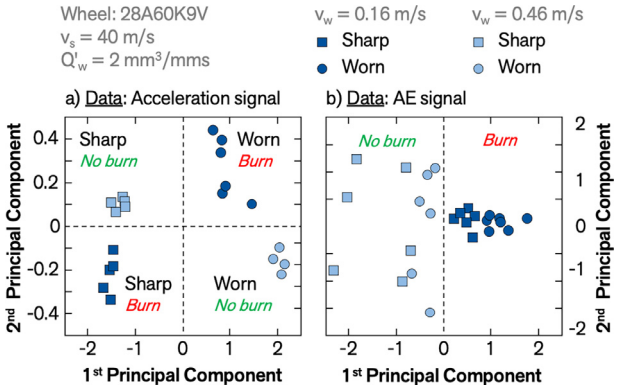


**Fig. 25.** Clustering different grinding conditions with PCA [174].

for feature extraction using accelerometer and AE signals, coupled with Principal Component Analysis (PCA), was analyzed in [174] to classify two wear states and differentiate between grinding burn and no burn with sharp and worn wheel. The analysis of the AE signal (Fig. 25b) enabled the differentiation between workpieces without grinding burn at higher workpiece speeds and workpieces with grinding burn at lower workpiece speeds. Notably, analysis of the acceleration signal also allowed for clustering of wear conditions (Fig. 25a).

Contrary to previous wheel-wear classification models, a regression model was introduced to predict the wear of a grinding wheel [296]. Here, the wear rate was calculated based on the maximum roughness of the grinding wheel at the start and the minimum roughness at the end of the grinding wheel's life. Spindle power, acceleration and AE signals were recorded. During feature extraction, features from the time, frequency, and time-frequency domains were calculated. Feature selection was then performed by excluding features that yielded low coefficients of determination $R^2$ when considered individually.

### 4.2. Data-driven detection of grinding burn

Data-driven identification of grinding burn offers the potential for indirect inspection of workpieces for grinding burn. In particular, the AE signal emitted during grinding can be used to detect damage at an early stage and avoid scrap [57]. When integrated into a monitoring system, it could enable real-time monitoring of industrial grinding processes.

Approaches for detecting grinding burn without the use of ML models were already developed as early as the 1980s and 1990s [94,270]. It was established that the AE signal is effective for grinding burn identification. The most informative frequency range was 100–300 kHz [94]. An ANN for in-process detection of grinding burn in surface grinding was developed [267] considering different feature sets for model input but lacking specific feature selection or evaluation by statistical parameters. Later, data acquisition was extended to include the recording of spindle power, providing two features – spindle power and AE signal – to an ANN for grinding-burn identification [173]. On the AE side, the maximum peak height from a FFT and the RMS signal were determined. Grinding burn was further classified based on AE signals and a Genetic Programming (GP) classifier, utilizing independent component analysis as the feature-selection method [111]. Additional studies investigated both AE and acceleration signals, using a FFT to determine the difference in frequency bands between workpieces with and without grinding burn [97]. For the AE signal, nine frequency bands ranging from 40 to 170 kHz, were identified. For acceleration, six frequency bands, ranging from 1 to 25 kHz, were identified. The raw data was filtered through a band-pass filter using these determined frequency bands as cutoff frequencies, in order to calculate the RMS signal for the input to the ML models. These results showed that the combination of AE and acceleration signals gave the best model results.

The impact of varying the depth of cut and feedrate on grinding burn was also studied [284]. Here, both accelerometer and AE signals were considered. Feature extraction entailed determining the spectral centroid of each raw signal via FFT and RMS value of the coefficients from the wavelet transform. The results showed a distinct advantage of the AE signal over the acceleration signal. However, the accuracy of the SVM model decreased when different feedrates were used. A follow-up study demonstrated the suitability of the Hilbert-Huang transform for signal analysis [285] and proposed a model to classify four grinding-burn stages while considering different feedrates and wheel speeds [239].

The AE signals from a spindle-integrated sensor and tailstock-mounted sensor were examined. The spindle current was also recorded as an RMS signal (*Irms*). For the SVM model, statistical features from the time domain as well as from various time-frequency transforms (PSD, STFT, WPT, EEMD, and VMD) (see Fig. 26) were utilized. These features were compiled into a feature vector $F_i$, serving as the model input. The accuracy of the model was then assessed based on these different signal features. Distinctions were made between the training results (CV score) and test results (test score). In both cases, the tailstock-mounted AE sensor underperformed compared to the spindle-integrated sensor due to the distance and intervening components between the emission source and the tailstock-mounted sensor. However, integrating all signals provided the highest model accuracy in both the training and validation phases.

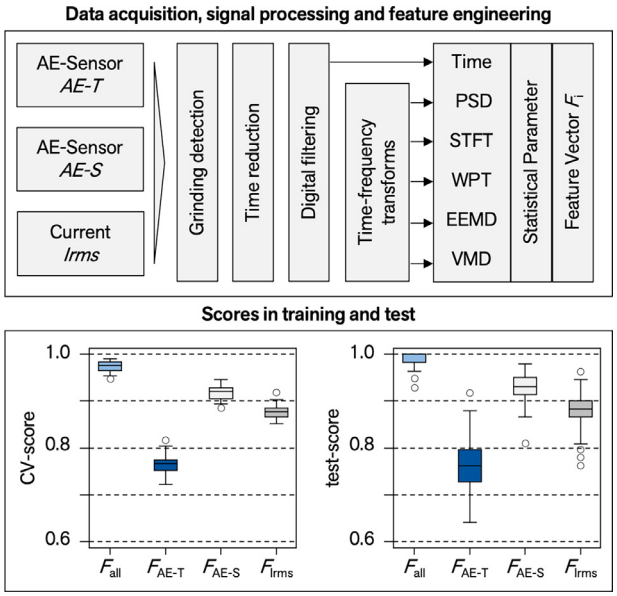


**Fig. 26.** Data acquisition and modeling of grinding burn [239].

### 4.3. Data-driven roughness prediction

In addition to workpiece dimensional and form tolerances, the surface roughness is also a critical factor in quality control. It is quantified by parameters such as the maximum-height roughness *Rz* or the arithmetic mean-height roughness *Ra*. Measurements are typically made away from the grinding machine using tactile measuring methods or confocal laser microscopy. However, it is also possible to measure roughness values in-machine using scattered light sensors. Also, data-driven modeling and monitoring offer the potential for indirect roughness predictions via sensor data and machine-control data. This offers the opportunity to identify rejects early and reduce measurement time, circumventing the need for costly sensor technology that is susceptible to environmental disruptions.

A non-linear stochastic differential equation model was used to extract sensor data and predict *Ra* surface roughness in grinding

[218]. The extraction of process features from vibration signals and the use of various ML methods for predicting *Ra* were explored in [41]. Furthermore, one of the first applications of active learning that leverages minimal experimental data (vibration signals) to predict surface roughness was presented in [40]. Another study investigated the suitability of using AE and power signals as inputs for ANNs in predicting workpiece *Ra* roughness during surface grinding [5]. Here, grinding tests were conducted with various infeeds, while the AE signal near the workpiece and the spindle power were recorded. A sampling rate of 1 MHz was chosen, and 50 kHz high-pass filter was used. For model input, two custom statistical parameters were tested: (i) the DPO parameter, i.e., the standard deviation of the RMS-AE signal multiplied by the maximum spindle power; and (ii) the DPKS parameter, which is the sum of the difference (to the fourth power) between spindle power and standard deviation of the spindle power multiplied by the standard deviation of the RMS-AE signal. During validation, the suitability of the combined signal source combination was also established. However, with increasing infeed (and thus increasing roughness), the model errors also increased.

A different approach for monitoring the workpiece roughness during surface grinding was developed by [212]. Here, measured values of normal and tangential grinding forces were used to predict *Ra*. The approach used a hybrid model that combined an Adaptive Neuro-Fuzzy Inference System (ANFIS) and a Gaussian Process Regression (GPR) to determine the grinding-wheel wear and workpiece surface roughness. The data for the models was sourced from grinding tests performed with various grit sizes, wheel speeds and infeeds.

In [210], researchers employed ANN as a regression model to determine surface roughness, utilizing a combination of grinding parameters and signal characteristics. To determine the features of the AE signals, the raw signal was obtained during surface grinding and then filtered using a bandpass filter, with additional noise suppressed by a discrete wavelet transform. In other words, wavelets localized features in the signal to different scales, allowing the preservation of important signal features while removing noise. From this pre-processed signal, two features were identified for use in the neural network: the maxima from the signal itself and the maxima from the RMS signal. [121] represents one of the first applications of Explainable AI (XAI) in establishing the DAQ scheme for surface-roughness prediction using vibration signals.

### 4.4. Data-driven process diagnostics

Data-driven models also have other applications. For example, process instabilities (such as vibration) and process input variables (such as wheel or work-material properties) can be detected. One such method was developed to classify the grinding-process variables with respect to the preceding turning operation (see Fig. 27) [32]. It demonstrated that the turning operation significantly affects the subsequent grinding process and its outputs. For example, when turning was done with a worn tool or without the finishing sequence, the deviations in shaft diameters after grinding were larger. The PCA of the grinding roughing and finishing sequence shown in Fig. 27 represents the dimensional reduction of selected time-series features of the RMS AE signal. The PCA shows clear clusters for the different groups, especially for the grinding roughing operation.

The findings highlight the interdependencies of successive manufacturing processes within a production chain. In general, the evaluation of machine-control and sensor data offers the potential to identify anomalies in the roughing stage, based on deviations from reference values, and then make adjustments in the finishing pass in order to maintain workpiece tolerances. Moreover, it is also possible to respond to changes that are influenced by the changes in materials or tools. For example, implementing data-driven grinding process control offers the potential to compensate for fluctuations within batches of incoming material blanks or when using different grinding wheels.

It is worth noting that the accuracy and applicability of data-driven models in the described use cases are highly dependent on specific grinding-system variables, such as work material, wheel type, grit size, and the process parameters used during model training. Consequently, altering any of these variables, such as switching the grinding wheel, may require fine-tuning or retraining of the model to maintain its accuracy.

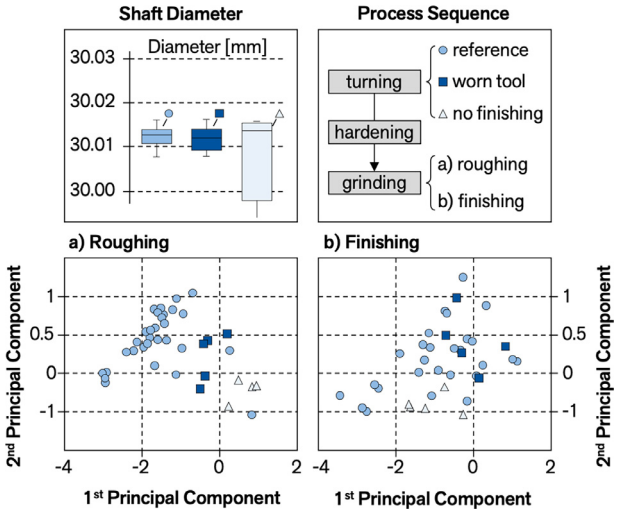


**Fig. 27.** Classification of process input variables [32].

## 5. Applications of modeling

Grinding models have advanced from theoretical academic research into practical simulation tools that are capable of analyzing defects, predicting grinding performance and optimizing processes for higher quality and productivity in real-world production. To demonstrate the practical applications and impacts of these models, several case studies are presented here, where the models are demonstrated to yield tangible impacts and are still actively used in industry. Specifically, the following successfully implemented use cases are examined: (i) General Motors, Timken, and RTX / Pratt & Whitney, using the GRINDsim® software developed by the late Stephen Malkin; (ii) industry partners of the WZL RWTH Aachen Gear Center using the GearGRIND3D® software, and end-users of Reishauer's gear-grinding machines; (iii) SKF, for bearing ring and ball grinding; (iv) Scania, for camshaft and crankshaft grinding; (v) Rush Machinery, for diamond-wheel truing; and (vi) Danobat Estarta and Advanced Finishing Technology (AFT), for centerless grinding.

### 5.1. GRINDsim® at GM, Timken Company, and Pratt & Whitney

The GRINDsim® simulation software utilizes the kinematics of grit-workpiece interaction and considers the curvature effects found in cylindrical grinding, shoulder grinding, cam-lobe grinding, crankpin grinding, gear grinding, and turbine blade root grinding [202]. The normal and tangential grinding forces are estimated by incorporating the sliding, plowing and chip-formation components. The model constants are determined through calibration, linking measured force/power to macro-scale wheel curvatures, micro-scale grit shapes and process parameters.

Fig. 28 illustrates the three major modules of GRINDsim®: (i) calibration, (ii) simulation, and (iii) optimization, using cam-lobe grinding as an example. The calibration module employs experimental measurements, such as power and quality inspections from grinding calibration tests, to find model constants depending on the wheel, work material, and process parameters. The accuracy of the simulation module's predictions heavily relies on this calibration.

The simulation module acts as a virtual grinder, taking inputs of the grinding wheel (geometry, abrasive, grade, and sharpness/dressing); the workpiece (material and shape); the process parameters (wheel speed, feedrate, etc.); and a database (based on results from the calibration module, which also contains mechanical and thermal

Please cite this article as: P. Krajnik et al., Advances in modeling of fixed-abrasive processes, CIRP Annals - Manufacturing Technology (2024), https://doi.org/10.1016/j.cirp.2024.05.001

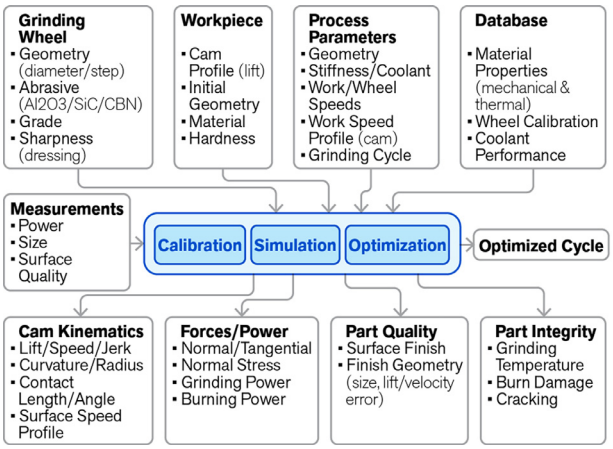


**Fig. 28.** Configuration of the GRINDsim® grinding simulation software.

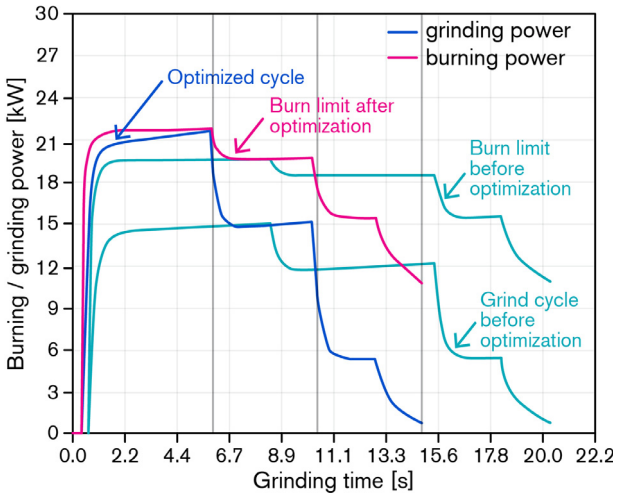


**Fig. 29.** Simulation of burning and grinding power plotted vs. time for infeed centerless grinding of bearing rollers at Timken.

properties of the workpiece and grinding fluid). It estimates the wheel-workpiece contact kinematics, the forces/power, and the workpiece surface integrity (thermal damage, residual stress, surface roughness, and deflection-related deviation of shape/tolerance) within the virtual grinding cycle.

The optimization module is built upon the simulation module and considers aspects such as machine-axes limits (for velocity, acceleration, jerk) and requirements for the final product. It iteratively evaluates the grinding cycle to select the best grinding process parameters at each stage, with an aim to optimize productivity by minimizing cycle time. In an optimal cycle for cam-lobe grinding, the virtual grinder will maximize the stock-removal rate during the roughing stage – while meeting constraints such as thermal damage, residual stress and surface quality requirements. During the finishing stage and spark-out, the desired surface roughness or final workpiece shape will be achieved. This software has been used to design, validate and optimize grinding processes in production by companies such as: General Motors (GM), for camshaft, crankshaft, and combustion-deck (cylinder-head) surface grinding [144]; Timken, for bearing ring grinding; and RTX/Pratt & Whitney, for grinding of turbine blade root [116] and turbine disk grooves [117,118].

An example of the GRINDsim® application can be seen in the use of a metal-bond, single-layer, electroplated cBN wheel in GM for grinding nodular cast iron camshafts. Using the simulation, this wheel has demonstrated consistent wheel life for about 200,000 to 400,000 parts with minimal wear. Another example is the planning of a camshaft grinding line in GM's Bay City, Michigan plant. The machine-tool supplier (Landis) estimated the need for 14 cam-lobe grinders. However, the software prediction indicated that only 10 machines would suffice. Consequently, the plant management decided to purchase 12 machines, resulting in a saving of about $1,000,000 per camshaft grinding machine.

The fatigue performance of bearings depends on the surface integrity generated by the grinding process. The selection of grinding and dressing parameters is crucial for managing the workpiece surface temperature to prevent grinding burn. Timken used GRINDsim® to optimize parameters in a bearing-ring grinding process so that the grinding power during roughing was just below the burning power limit.

Fig. 29 provides an example of an OD shoe-centerless grinding cycle applied to 60 mm diameter AISI 52100 steel rollers. In the finish and spark-out stages, GRINDsim® was used to choose parameters that kept power well below the burn limit. This reduced cycle time by 25 %.

At RTX / Pratt & Whitney, model-based simulation of continuous-dress creep-feed grinding was used to avoid thermal damage and cracking of the thermal barrier coating (caused by thermal strain) for turbine blade root serration grinding. This was achieved by adjusting the workpiece speed and the dressing infeed [116]. The implementation demonstrated a 40 % reduction in cycle time while keeping heat flux and grinding forces (calculated based on in-process power measurements) below critical values. The input parameters were then adaptively controlled to minimize cycle time [117]. Additionally, the grinding simulation was extended to single-layer electroplated cBN grinding wheels for disk slots made of nickel-based superalloy. When grinding with electroplated wheels, grinding power (and therefore heat) increases as the wheel wears. Therefore, worn wheels were used during validation. GRINDsim® was used to establish and validate a power model to prevent the formation of a white layer caused by high workpiece temperature [118]. In addition, this model was applied to simulate the 5-axis grinding of fir tree-shaped grooves in turbine disks using small, single-layer electroplated cBN wheels. The aim was to prevent thermal damage to the workpiece and premature wheel failure. Finally, the model was used to predict forces, power, heat flux and temperature, which were then utilized in a multi-constraint optimization to reduce cycle time [119].

### 5.2. Applications in gear grinding (GearGRIND3D® and ARGUS)

GearGRIND3D is a simulation program specifically developed for gear grinding. An overview is shown in Fig. 30. Modeling of gear grinding is challenging due to the complex contact conditions (geometry) at the wheel-workpiece interface. At WZL RWTH Aachen, simulations have been developed for different gear-grinding processes based on numerical penetration calculations.

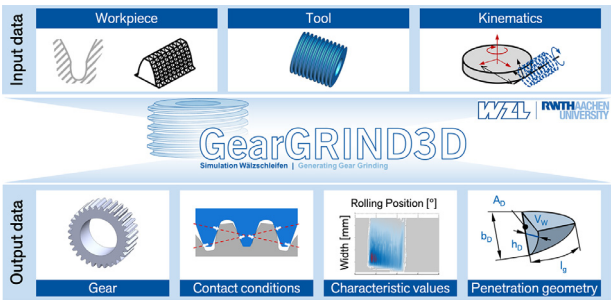


**Fig. 30.** Configuration of the GearGRIND3D simulation.

The principle behind the penetration calculation involves bringing ideal geometries of the tool, abrasive grit and workpiece into contact and superimposing them incrementally based on process kinematics. The contact path of the abrasive grit through the workpiece corresponds to the undeformed penetrated volume. Using these penetration calculations with the process kinematics and workpiece and tool

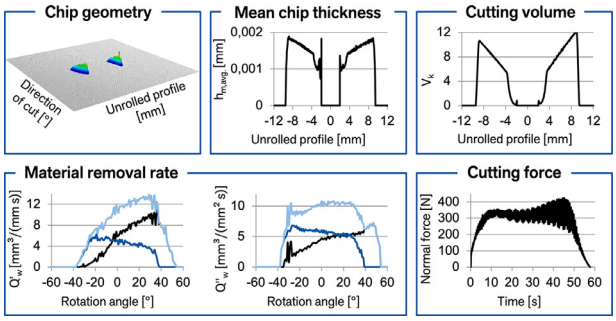


**Fig. 31.** Grinding force model for continuous generating gear grinding (based on [136,273]).

geometry, optimal process parameters are determined. An example is shown in Fig. 31 for continuous-generating gear grinding.

Grinding forces are key factors in evaluating grinding processes. Numerous models for predicting grinding forces rely on process parameters, geometry and kinematics in the contact zone [255,273]. A model was integrated into GearGRIND3D simulation to calculate the grinding force for generating gear grinding considering the chip geometry and empirical constants determined by grinding tests [136]. Here, macro simulations were combined with microscopic grit penetration, which necessitates the determination of the chip's cross-sectional area and the number of kinematic cutting edges. The predicted and measured forces showed a strong correlation [240].

The specific grinding energy is necessary for determining the mechanical and thermal load. It is calculated based on three phases of grit-workpiece contact: sliding (friction), plowing, and chip-formation (shearing), as shown in Fig. 32 [184]. The wheel topography was integrated into the simulation [67], and the interactions between individual grits and the work material, as well as the resulting chip, were modeled to calculate individual energy contributions for each grit. The cutting energy required for material removal was determined by multiplying the cutting force $F_c$, the cutting speed $v_c$, and the contact time $t_k$. [252].

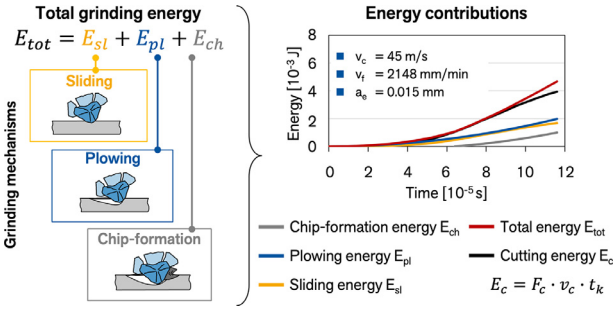


**Fig. 32.** Grinding energy model for continuous generating gear grinding (adapted from [184,252]).

While GearGRIND3D serves as an example of software that integrates a variety of process models for process planning, there is a growing need to extend the models for real-time process and condition monitoring. In this context, the ARGUS Monitoring System by Reishauer is a good example, highlighting the integration of physical and data-driven models into a cloud platform that paves the way for simultaneous condition monitoring of multiple machines in various manufacturing plants. [77,78] demonstrated that continuous-generating gear grinding processes can be optimized via the application of nonlinear models for the normal $F_n$ and cutting $F_c$ forces, as:

$$F_n = F_{n0} + k\left(\frac{a_e v_f}{v_c}\right)^{\varepsilon} l_k^{\varphi} a_p \tag{17}$$

$$F_c = \mu F_n \tag{18}$$

where the chip geometry is determined by the depth $a_e$, width $a_p$, and length $l_k$ of cut and the process kinematics is determined by the feedrate $v_f$ and the cutting speed $v_c$. The minimal-normal-force $F_{n0}$, the coefficient $k$, and exponents $\varepsilon$ and $\varphi$ must be experimentally determined via an iterative fitting that uses measurements of forces or spindle power. Upon establishing these values, the ARGUS Monitoring System can carry out real-time compensation. This compensation is critical in addressing small-force variations. The force model is recalculated every time the worm diameter changes due to dressing. Most importantly, the system is able to predict the kinematic roughness, taking into account the vibration (dynamic) properties of the machine.

### 5.3. SKF's BEAring Simulation Tool (BEAST)

BEAST is a 3D multibody simulation tool developed by SKF to simulate bearing dynamics and dynamics of grinding systems that consist of rigid and/or flexible bodies connected by compliant joints. It solves differential equations of motion and mechano-tribological phenomena at the contact interfaces. The model-body geometries can be built from scratch or imported as a CAD file. The joints (or connections between the bodies) have specific/assigned stiffness and damping. The models were developed using an object-oriented extension of Mathematica [9].

In cases were rings have a low ratio of wall thickness to diameter, the dynamic stiffness is low. Therefore, part distortion from grinding forces is likely. For shoe-centerless grinding of bearing rings with low dynamic stiffness, BEAST was successfully used to simulate and optimize this complex process. In addition, BEAST was used to optimize shoe design and develop a strategy to cancel out low-order waviness from incoming rings. This necessitated modeling the machine-structure eigenfrequencies, wheel out-of-balance, clamping forces, friction in support shoes, etc.

BEAST was also used to simulate the kinematics in finishing of silicon nitride balls [171]. In this operation, the geometry of the diamond-plate groove and the orbital motion both have a distinct influence on the material removal and, therefore, need to be modeled. Fig. 33 shows the simulation of ball grinding where the ball cage in the rotating table forces the balls to move with the same speed and fixed spacing while the balls are constrained in the abrasive groove. The contact-dynamics model aided in simulating the density of contacts between the ball surface and the abrasive tool (Fig. 33d), material-removal distribution (Fig. 33c) with the X-axis representing circumferential positions on the ball, the Y-axis indicating positions from pole-to-pole, and the Z-axis showing material removal depth, as well as the time needed to achieve an even distribution of contacts. This aided the optimization of tool design and process parameters, especially when the incoming blanks differed in size and had a non-spherical shape.

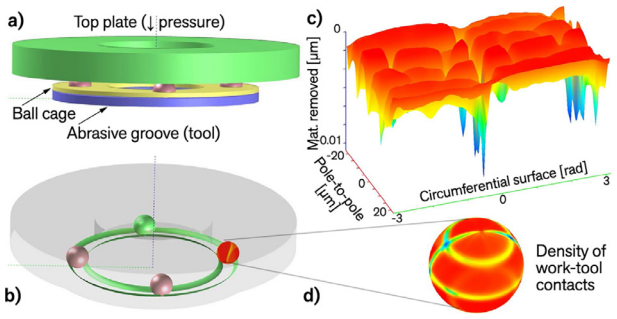


**Fig. 33.** BEAST simulation of ceramic ball-grinding [171].

The theory of aggressiveness [89] was implemented to model free-rotation double-disc grinding of bearing components with the goal of avoiding: (i) workpiece stoppage, which occurs at low free-rotation workpiece speeds; and (ii) thermal damage, which occurs at

Please cite this article as: P. Krajnik et al., Advances in modeling of fixed-abrasive processes, CIRP Annals - Manufacturing Technology (2024), https://doi.org/10.1016/j.cirp.2024.05.001

high workpiece speeds [85]. This analytical approach proved valuable in modeling the material removal in steady-state grinding. The BEAST, in contrast, is able to predict transient forces acting on the roller (workpiece) until a steady state was reached and also the sharp transition from high-speed roller spinning to roller stalling at high workpiece-coverage ratio.

### 5.4. Camshaft and crankshaft grinding simulation at Scania

The constant-temperature process for camshaft and crankshaft grinding has been implemented in Scania's production lines in Sweden and Brazil. Before implementation, the constant-temperature grinding process underwent a rigorous Production Part-Approval Process (PPAP) followed by patenting [161,167]. All model-based simulations were integrated with Excel and are used exclusively by Scania.

Camshaft grinding is a complex process due to the non-round shape of the workpiece [87]. Previous research on cylindrical grinding of non-round geometries has shown that cycle times can be significantly reduced by using thermal models to maintain workpiece temperatures just below the burn threshold [162]. This constant-temperature approach was successfully applied to the grinding of cam lobes [163], leading to a 20 % cycle-time reduction and a lower risk of thermal damage.

Grinding of crankshafts also poses a specific challenge due to the difficulty of grinding the sidewall. In this case, the contact length at the interface of the grinding wheel and sidewall increases, which significantly reduces the grinding aggressiveness. This reduction can lead to excessive temperatures. To prevent this issue, the concept of constant-temperature grinding was adapted [91]. The models developed for process geometry, kinematics, and thermal aspects allowed for the selection of "feed increments" that minimized wheel wear and kept the process below the burn threshold. The model identified the depth of cut during each workpiece revolution, enabling the algorithm to determine the increments in such a way that a predetermined burn threshold is matched at two critical contact points: on the radius and on the sidewall [167]. Fig. 34 illustrates the flowchart of the algorithm for the reverse calculation of grinding parameters from the wheel's final position to ensure constant workpiece temperature and maximum material-removal rate. This application resulted in a 25 % reduction in cycle time.

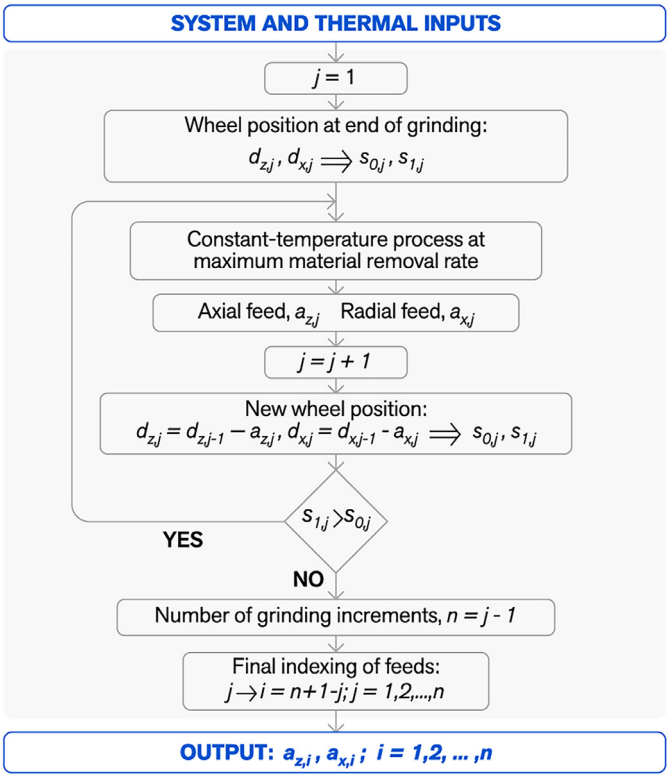


**Fig. 34.** Scania's temperature-controlled method for determining grinding parameters in crankshaft grinding [167].

### 5.5. Diamond wheel truing at rush machinery

The geometry and kinematics of truing diamond grinding wheels were analytically modeled by [86]. A fundamental relationship was established that relates the truing compliance number $\Gamma_T$ to the truing efficiency $\eta_T$, which encompasses truing parameters and truing $d_{g,T}$ and diamond $d_{g,D}$ grit sizes:

$$\Gamma_T = \left(\frac{d_{g,T}}{d_{g,D}}\right)^2 Aggr = \left(\frac{d_{g,T}}{d_{g,D}}\right)^2 \frac{1}{|1-q_T|}\sqrt{\frac{a_{T,eff}}{d_{eq}}} \tag{19}$$

$$\eta_T = \frac{\Delta r_d}{a_{T,eff}} \tag{20}$$

where the truing aggressiveness number accounts for the truing speed ratio $q_T$, the effective truing depth $a_{T,eff}$ and the equivalent diameter $d_{eq}$. $\Delta r_d$ is the reduction of the diamond wheel radius in the truing contact. These models were embedded in a Rush Machinery's software tool using HTML5 markup language for optimizing needs, such as shorter cycle times, less truing-wheel consumption, lower truing forces, or all the above. The online truing-parameters calculator [193] outputs the optimal parameters for the selected truing wheel and also suggests an optimal wheel, which can be ordered via an online link.

### 5.6. Applications in centerless grinding (SUA and Opt-Setup Master)

In 1964, the first application of computer simulation in centerless grinding was published [231]. Advances in modeling and simulation of plunge and throughfeed centerless grinding were reviewed in two CIRP keynote papers, first in 1989 [235] and later in 2012 [126]. However, many models – despite their advancement – have not been widely adopted in industrial applications, limiting their impact.

Some exceptions exist, such as a time-domain dynamic model of the instantaneous workpiece radius [27]. This model assists the cycle configuration of centerless grinding through continuous variable speed. Transitioning to model application, the Set-Up Assistant (SUA) is the latest software tool developed by Danobat Estarta. Designed for both plunge and throughfeed operations, SUA uses a combination of analytical and empirical models to simulate a variety of process parameters. Additionally, it includes heuristic algorithms within its optimization engine [29]. SUA is available as either an executable program in MATLAB or as a web platform (Fig. 35). The software contains input, calibration,

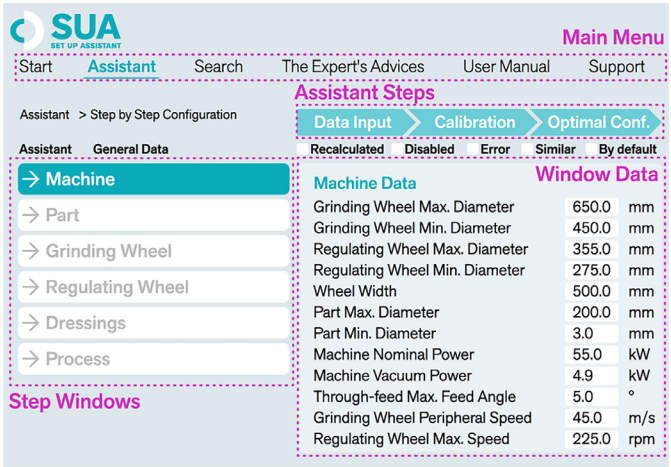


**Fig. 35.** Graphical user interface of Danobat Estarta's Set Up Assistant.

simulation and optimization modules, which are similar to those found in GRINDsim®. The simulation module includes simulations for process forces, power, part diameter, roundness, straightness, thermal damage, roughness, and stability charts. The optimization module assists machine users in selecting a stable operational range for part height, blade angle, workpiece speed, and infeed speed based on stability criteria [25].

Hashimoto [123] developed a model-based simulation that integrates the three stability criteria: (i) work-rotation stability; (ii) geometrical-rounding stability; and (iii) dynamic-system stability [127]. The model is integrated into the Opt-Setup Master (Fig. 36), an Excel-based simulation that can aid an end-user to select optimum setup conditions to ensure safe operations, better roundness and chatter-free grinding. Additionally, a static grinding model was introduced in [124] for selecting operating conditions, e.g., feedrate, wheel speed, system stiffness (incl. wheel-contact stiffness based on a workpiece size). Opt-Setup Master by Advanced Finishing Technology (AFT) gives end users a practical tool for designing grinding cycles to control the size error, roundness error and cycle time. This software has been implemented in real centerless production located in United States, Japan, China, India and Romania.

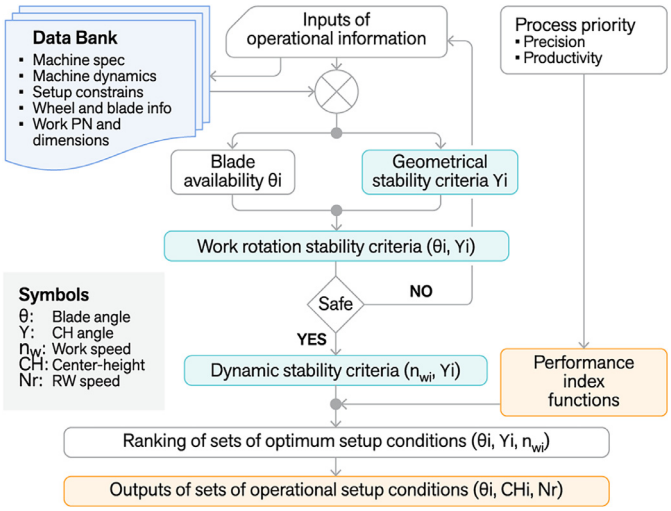


**Fig. 36.** Flow chart of the AFT's Opt-Setup Master [123].

## 6. Challenges and future directions

Early advances in scientific understanding of grinding processes were primarily made through experiments. Foundational models such as specific energy and maximum undeformed chip thickness, established 70 years ago, remain integral to grinding research today. The equivalent-chip-thickness model, promoted by the CIRP keynote in 1974 [246], is still in use as well despite its limitations to fully account for process geometry and kinematics, particularly when contrasted with more fundamental dimensionless parameters such as the aggressiveness number.

Basic empirical models (e.g. regression for curve fitting) have been experiencing a steady decline since 1992. Although these models can be useful for optimizing a specific set of grinding conditions, they insufficiently advance the fundamental understanding of the process mechanics. Their reliance on measured values constrains their utility to the original conditions under which they were developed, making them difficult to apply under different boundary conditions. Moreover, the experimental effort required to determine model constants increases exponentially with the addition of variables [255]. Therefore, experiments are often complemented with modeling. For example, while research which produces new experimental data – such as the impact of dresser direction on the efficiency of grinding-wheel dressing [151] – is useful knowledge and valuable to practitioners, it does not enhance the understanding of process mechanics. In contrast, when novel insights are uncovered – for example, into dressing mechanics [21] – and coupled with experimental data, this research gives universal applicability which can be extrapolated to other wheel-conditioning applications. In other words, models that not only showcase experimental findings but also interpret these results through the lens of first principles produce more value.

While macro-scale models capture process geometry and kinematics and are proven capable of optimizing a wide variety of fixed-abrasive processes, micro-scale models are necessary to comprehensively address interface interactions (Fig. 7) and the intricate thermomechanical aspects crucial for understanding material removal, wear and surface-finish formation. The key input to micro-scale models is the wheel topography. Early studies of wheel topography and related empirical parameters mostly originated in Germany [153,223,273]. These models require measuring and quantifying the wheel topography, such as the cutting-point density $C$, which is a key parameter in the calculation of the maximum undeformed chip thickness (Eq. (3)) [16]. Although numerous methods have been developed for quantifying the wheel topography, this remains a challenge – especially for practitioners with limited access to optical imaging instruments.

The convergence of micro- and macro-scale models presents both challenges and opportunities for future research. Key challenges include accurately capturing the complex, dynamic interactions at the micro-scale – such as grit-workpiece contact –and integrating these into macro-scale models. Future research could focus on enhancing the fidelity of micro-scale models, improving the integration methods for scaling up to macro-scale, and improving computational techniques to manage the increased complexity. The integration of models into simulation has become easier thanks to advancements in hardware (computational speed and memory), along with software enhancements, which together enable the creation of dedicated simulation tools. Such software has effectively demonstrated its ability to incorporate a large variety of models, which can include kinematics, wheel and workpiece topography, material-removal mechanisms, friction, wear, fluid flow, and heat transfer. It is also capable of addressing the micro-scale effects of abrasive interactions between the wheel and the workpiece. Micro-geometric effects, however, continue to pose a significant challenge, largely due to the stochastic nature of the wheel topography, which needs to be included into process models. Although modern optical tools can characterize the wheel topography and provide comprehensive 3D data, the primary difficulty lies in translating this 3D data into tool descriptors for simulation and vice versa.

Developing a comprehensive physical model necessitates the use of field equations, which involve partial differential equations. The discretization methods utilized include FEM, SPH, MD, CFD, FV, and dexels. SPH offers benefits for representing material separation, but it necessitates a consistent second derivative for the heat-transfer equation as well as some corrections and stabilizations. The key requirement and obstacle for all these models are the constitutive equations for the work material and friction model, specifically the acquisition of model parameters. Due to the extreme conditions present during the process, standard material testing may not yield sufficient results. Promising techniques include the use of instrumented scratch tests or orthogonal-cutting experiments.

Wear modeling remains insufficiently developed as no existing model takes into account the full effect chain of wear and loading, and there is no combined model capable of predicting workpiece properties through the dressing and grinding processes.

Further research is needed to understand the interaction between grinding fluid and the grinding wheel as well as the heat-transfer mechanisms within the wheel-workpiece contact zone. These interactions affect the heat partition to the workpiece, grinding wheel, chips and fluid. Knowing these heat partitions is

Please cite this article as: P. Krajnik et al., Advances in modeling of fixed-abrasive processes, CIRP Annals - Manufacturing Technology (2024), https://doi.org/10.1016/j.cirp.2024.05.001

required for accurate thermal models. Thermal models have evolved, incorporating CFD simulations to account for a variety of boundary conditions. Further refinement and experimentation could improve their accuracy. A solution to this complexity may require the integration of thermal analysis with models that consider material physics and the resulting surface integrity outputs. Modeling fluid flow is a complex task which includes addressing the surface properties of the grinding wheel, multi-phase flow, heat distribution among different constituents, and the dynamic heat transfer coefficient. Two-dimensional fluid flow simulations do not provide sufficiently accurate results; three-dimensional simulations of fluid flow are expected to become more feasible with the continuous advancement in computing power.

Aided by advances in computers and process monitoring, data-driven models are rapidly gaining prominence. This represents a significant shift from the traditional approach to modeling. Most data-driven models use supervised machine learning (ML), which is highly process-dependent and sensitive to variations in process parameters, limiting their transferability. Acceleration and acoustic emission (AE) sensors are primarily used, with AE sensors generally showing better utility. For AE sensors, the challenge remains in determining their optimal positioning. Correct positioning of the sensor relative to the emitting source and processing the raw signals by filtering specific frequency bands can improve the model accuracy. Combining multiple signal sources for feature extraction (through sensor fusion) demonstrated potential for improving data-driven models. It is important to note that the sensor-fusion solutions remain underexplored, presenting an important avenue for further research. Support Vector Machine (SVM) approaches often outperform Artificial Neural Networks (ANN) on relatively small data sets, although they require significant computational effort. Modern approaches integrate multiple signal sources, a trend that is expected to continue. Improving the transferability of data-driven models is key to ensure a broader applicability. There is a current need for more models that provide time-continuous predictions of tool wear and surface roughness, as well as models that can identify and compensate for disturbances within the grinding process. This is especially crucial for honing and superfinishing operations, where the tool-wear behavior is less understood, akin to a "black box". In this context, physics-informed ML appears to be a promising future direction. This approach may overcome the limitations of data-driven models by enhancing their ability to extrapolate across different conditions without being strictly dependent on datasets that match the process parameters. The accuracy of data-driven models depends on the quality and volume of data. Integrating data-driven and physical models [238] could improve their alignment with the underlying process physics and reduce the need for extensive empirical calibration by filtering out data inconsistencies that diverge from expected physical behaviors. Such a hybrid approach not only facilitates the development of more accurate models, but also paves the way for research directions in sensor integration and process monitoring.

Simulation of fixed-abrasive operations for process and product design has been adopted slowly and steadily in the industry as an important part of the digital twin for smart factories and manufacturing operations. Accurate modeling of a complex grinding process, with a short lead time for the modeling phase, remains technically challenging due to the ongoing advancements in abrasives and wheel bonding, coupled with more stringent engineering specifications (such as durability and reliability). The calibration of simulation models needs to be carefully considered. Fortunately, the increasing availability of data obtained by process monitoring facilitates this calibration process, making it more feasible to achieve high levels of accuracy in simulations. Modeling and simulation significantly contribute to reductions in costs, cycle time and scrap – consequently reducing the ecological footprint of grinding. Efforts to simulate abrasive machining processes, grinding in particular, have persisted over the past decades and, based on the trend observed, are continuing and will continue to transform the modeling of fixed-abrasive processes. In addition, the synergy between modeling and simulation, process monitoring, and intelligent control needs to be further developed to optimize process parameters in real-time, responding to variations in process conditions to maintain optimal performance.

Furthermore, it is crucial to address the current gap in simulations related to dressing, as there is a lack of comprehensive models that consider the impact of the dressing process. This gap in modeling limits our understanding of how dressing affects the grinding process, which ultimately impacts the properties of the workpiece.

## 7. Concluding remarks

The seminal models developed by Shaw, Pahlitzsch, Peklenik, Werner, Malkin, and others continue to hold relevance and are the cornerstone of fundamental knowledge in the field. These physical models offer a comprehensive understanding of process mechanics and are fast to deploy. As a result, they serve as the basis for industrial simulations, facilitating robust process prediction and optimization.

The evolution in modeling from 1992 to 2006 to 2024 has been marked by advancements in model capabilities and applications. Over time, the scope of modeling has broadened to include a diverse sub-array of modeling approaches, such as FEM, MD, ANN, and SPH. This diversification was driven by the need to address the increasing complexity of abrasive processes, especially in terms of accounting for micro-scale effects.

Thermomechanical modeling with integrated process geometry and kinematics remains a key pillar for predicting material removal, forces, wear, temperatures and surface integrity. The accuracy of these models has been improved by leveraging advancements in computational techniques and the inclusion of improved material constitutive models.

Empirical models can be highly predictive within the domain of the data they are based on. Advances in data-driven approaches, with ML playing a major role, are also evident. The increasing availability of process data across various time scales further highlights this trend. The increasing prospects of leveraging edge and cloud computing with data-driven approaches will enhance the availability of simulation tools. Furthermore, integrating physical models with data-driven (e.g. ML) models and physics-informed AI models show great promise. Each modeling approach offers certain advantages, depending on the goals and the specific process aspects being investigated.

Drawing on the CIRP's fifty-year legacy in modeling of abrasive operations, this paper aligns with the tradition of providing critical reviews every 15–20 years, setting the stage for the continuation of the research endeavors in this subject area.

## Declaration of competing interest

The authors declare that they have no known competing financial interests or personal relationships that could have appeared to influence the work reported in this paper.

## CRediT authorship contribution statement

**Peter Krajnik:** Writing – review & editing, Writing – original draft, Visualization, Project administration, Methodology, Conceptualization. **Konrad Wegener:** Writing – review & editing, Writing – original draft, Visualization, Supervision, Methodology, Conceptualization. **Thomas Bergs:** Writing – review & editing, Writing – original draft, Visualization, Supervision, Methodology, Conceptualization. **Albert J. Shih:** Writing – review & editing, Writing – original draft, Visualization, Methodology, Conceptualization.

## Acknowledgments

The authors thank J. Badger (3), D. Barrenetxea (2), P. Breuer, S. Bukkapatnam (2), R. Chaudhari, C. Dietz, W. Graf, C. Guo (1), T. Gustavsson, F. Hashimoto (1), B. Kirch, A. Klink (2), M. Kuffa, A. Malakizadi, E. Reuter, B. Rowe (1), P. Wiederkehr (2), and G. Xiao for their contribution to this paper.

## References

[1] Adibi H, Rezaei SM, Sarhan AAD (2013) Analytical Modeling of Grinding Wheel Loading Phenomena. *The International Journal of Advanced Manufacturing Technology* 68(1):473–485.
[2] Afrasiabi M, Meier L, Röthlin M, Klippel H, Wegener K (2020) GPU-Accelerated Meshfree Simulations for Parameter Identification of a Friction Model in Metal Machining. *International Journal of Mechanical Sciences* 176:105571.
[3] Agarwal S (2019) On the Mechanism and Mechanics of Wheel Loading in Grinding. *Journal of Manufacturing Processes* 41:36–47.
[4] Agarwal S, Paruchuri VR (2012) Predictive Modeling of Undeformed Chip Thickness in Ceramic Grinding. *International Journal of Machine Tools and Manufacture* 56:59–68.
[5] Aguiar PR, Cruz CED, Paula WCF, Bianchi EC (2008) *Predicting Surface Roughness in Grinding Using Neural Networks*, InTech, Rijeka, Croatia, 33–44.
[6] Akbari M, Buhl S, Leinenbach C, Wegener K (2016) A New Value for Johnson Cook Damage Limit Criterion in Machining with Large Negative Rake Angle as Basis for Understanding of Grinding. *Journal of Materials Processing Technology* 234:58–71.
[7] Alden G (1914) Operation of Grinding Wheels in Machine Grinding. *Transactions of the ASME* 36:451–460.
[8] Alpaydın E (2020) *Introduction to Machine Learning*, MIT PressCambridge, USA.
[9] Anders J, Leslie P, Stacke L-E (2013) Rotor Drop Simulations and Validation with Focus on Internal Contact Mechanisms of Hybrid Ball Bearings. *In: ASME Turbo Expo*, San Antonio, USA. V07BT30A027.
[10] Araujo LM, Esteves PB, Fabbro S, Kuffa M, Wegener K (2023) Geometric-Kinematic Model for Wear Simulation of Diamond-Impregnated Segments in Concrete Core Drilling. *Procedia CIRP* 117:38–43.
[11] Archard JF (1953) Contact and Rubbing of Flat Surfaces. *Journal of Applied Physics* 24(8):981–988.
[12] Arun A, Krishnaswamy R, Unnikrishnan D, Sumesh A (2018) Tool Condition Monitoring of Cylindrical Grinding Process Using Acoustic Emission Sensor. *Materials Today: Proceedings* 5:11888–11899.
[13] Aurich J, Sudermann H, Braun O (2006) Experimental Investigation of Burr Formation in the Surface Grinding of Tool Steel. *Proceedings of the Institution of Mechanical Engineers, Part B: Journal of Engineering Manufacture* 220 (4):489–497.
[14] Aurich JC, Biermann D, Blum H, Brecher C, Carstensen C, Denkena B, Klocke F, Kröger M, Steinmann P, Weinert K (2009) Modelling and Simulation of Process: Machine Interaction in Grinding. *Production Engineering* 3(1):111–120.
[15] Aurich JC, Kirsch B (2012) Kinematic Simulation of High-Performance Grinding for Analysis of Chip Parameters of Single Grains. *CIRP Journal of Manufacturing Science and Technology* 5(3):164–174.
[16] Backer WR, Marshall ER, Shaw MC (1952) The Size Effect in Metal Cutting. *Transactions of the ASME* 74(1):61–71.
[17] Backer WR, Merchant ME (1958) On the Basic Mechanics of the Grinding Process. *Transactions of the ASME* 80(1):141–146.
[18] Badger J (2008) Practical Application of Aggressiveness and Chip Thickness in Grinding. *In: 3rd CIRP International Conference on High Performance Cutting (HPC)*, Dublin, Ireland, 599–606.
[19] Badger J, Drazumeric R, Krajnik P (2016) Grinding of Cermets with Cup-Wheels. *Materials Science Forum* 874:115–123.
[20] Badger J, Drazumeric R, Krajnik P (2021) Application of the Dimensionless Aggressiveness Number in Abrasive Processes. *Procedia CIRP* 102:361–368.
[21] Badger J, Hoier P, Vindemmio S, Nigro F, Drazumeric R, Krajnik P (2023) On Mechanics and Monitoring of Plunge-Roll Rotary Dressing of Grinding Wheels. *CIRP Annals* 72(1):277–280.
[22] Badger J, Murphy S, O'Donnell G (2011) The Effect of Wheel Eccentricity and Run-out on Grinding Forces, Waviness, Wheel Wear and Chatter. *International Journal of Machine Tools and Manufacture* 51(10):766–774.
[23] Badisch E, Varga M, Eder SJ (2019) A Brief Review of Abrasive Wear Modelling Using a Numerical-Experimental Approach. *Key Engineering Materials* 799:83–88.
[24] Barandas M, Folgado D, Fernandes L, Santos S, Abreu M, Bota P, Liu H, Schultz T, Gamboa H (2020) TSFEL: Time Series Feature Extraction Library. *SoftwareX* 11:100456.
[25] Barrenetxea D, Alvarez J, Madariaga J, Gallego I (2011) Stability Analysis and Time Domain Simulation of Multiple Diameter Parts During Infeed Centerless Grinding. *CIRP Annals* 60(1):351–354.
[26] Barrenetxea D, Alvarez J, Marquinez JI, Gallego I, Muguerza Perello I, Krajnik P (2014) Stability Analysis and Optimization Algorithms for the Set-up of Infeed Centerless Grinding. *International Journal of Machine Tools and Manufacture* 84:17–32.
[27] Barrenetxea D, Alvarez J, Marquinez JI, Sanchez JA (2016) Grinding with Controlled Kinematics and Chip Removal. *CIRP Annals* 65(1):341–344.
[28] Barrenetxea D, Mancisidor I, Beudaert X, Munoa J (2018) Increased Productivity in Centerless Grinding Using Inertial Active Dampers. *CIRP Annals* 67(1):337–340.
[29] Barrenetxea D, Marquinez JI, Álvarez J, Fernández R, Gallego I, Madariaga J, Garitaonaindia I (2012) Model-Based Assistant Tool for the Setting-up and Optimization of Centerless Grinding Process. *Machining Science and Technology* 16 (4):501–523.
[30] Barwell FT (1958) Wear of Metals. *Wear* 1(4):317–332.
[31] Baumgart C, Radziwill JJ, Kuster F, Wegener K (2017) A Study of the Interaction between Coolant Jet Nozzle Flow and the Airflow around a Grinding Wheel in Cylindrical Grinding. *Procedia CIRP* 58:517–522.
[32] Beckers A, Hommen T, Becker M, Kornely MJK, Reuter E, Grünert G, Ortjohann L, Jacob J, Niemietz P, Barth S, Bergs T (2022) Digitalized Manufacturing Process Sequences – Foundations and Analysis of the Economic and Ecological Potential. *CIRP Journal of Manufacturing Science and Technology* 39:387–400.
[33] Bergs T (2018) Cutting Force Model for Gear Honing. *CIRP Annals* 67(1):53–56.
[34] Bergs T, Biermann D, Erkorkmaz K, M'Saoubi R (2023) Digital Twins for Cutting Processes. *CIRP Annals* 72(2):541–567.
[35] Bergs T, Hardt M, Schraknepper D (2019) Inverse Material Model Parameter Identification for Metal Cutting Simulations by Optimization Strategies. *In: 15th International Conference on High Speed Machining, Prague, Czechia*, 3172–3178.
[36] Bergs T, Röttger J, Barth S, Prinz S (2021) Approach to the Numerical Modelling of the Chip Temperatures in Single Grain Scratching. *Production Engineering* 15 (3):451–455.
[37] Biermann D, Blum H, Rademacher A, Scheidler AV, Weinert K (2012) Simulation of Process Machine Interaction in NC-Shape Grinding. *Process Machine Interactions, Lecture Notes in Production Engineering*, 121–141.
[38] Biermann D, Holtermann R, Menzel A, Schumann S (2016) Modelling and Simulation of Thermal Effects in Internal Traverse Grinding of Hardened Bearing Steel. *CIRP Annals* 65(1):321–324.
[39] Bifano TG, Fawcett SC (1991) Specific Grinding Energy as an In-Process Control Variable for Ductile-Regime Grinding. *Precision Engineering* 13(4):256–262.
[40] Botcha B, Iquebal AS, Bukkapatnam STS (2021) Efficient Manufacturing Processes and Performance Qualification via Active Learning: Application to a Cylindrical Plunge Grinding Platform. *Procedia Manufacturing* 53:716–725.
[41] Botcha B, Rajagopal V, Babu N, R, Bukkapatnam STS (2018) Process-Machine Interactions and a Multi-Sensor Fusion Approach to Predict Surface Roughness in Cylindrical Plunge Grinding Process. *Procedia Manufacturing* 26:700–711.
[42] Brecher C, Esser M, Witt S (2009) Interaction of Manufacturing Process and Machine Tool. *CIRP Annals* 58(2):588–607.
[43] Brecher C, Hermes R, Esser M (2013) HPC-Stability Simulation. *Process Machine Interactions, Lecture Notes in Production Engineering*, 179–202.
[44] Brinksmeier E, Aurich JC, Govekar E, Heinzel C, Hoffmeister HW, Klocke F, Peters J, Rentsch R, Stephenson DJ, Uhlmann E, Weinert K, Wittmann M (2006) Advances in Modeling and Simulation of Grinding Processes. *CIRP Annals* 55(2):667–696.
[45] Brinksmeier E, Çinar M (1995) Characterization of Dressing Processes by Determination of the Collision Number of the Abrasive Grits. *CIRP Annals* 44(1):299–304.
[46] Brinksmeier E, Gläbe R, Klocke F, Lucca DA (2011) Process Signatures – an Alternative Approach to Predicting Functional Workpiece Properties. *Procedia Engineering* 19:44–52.
[47] Buhl S, Leinenbach C, Spolenak R, Wegener K (2013) Failure Mechanisms and Cutting Characteristics of Brazed Single Diamond Grains. *The International Journal of Advanced Manufacturing Technology* 66(5):775–786.
[48] Buj I, Calvet J, Coba Salcedo MF (2010) Use of Roughness Probability Parameters to Quantify the Material Removed in Plateau-Honing. *International Journal of Machine Tools and Manufacture* 50:621–629.
[49] Cao J, Wu Y, Li J, Zhang Q (2016) Study on the Material Removal Process in Ultrasonic-Assisted Grinding of SiC Ceramics Using Smooth Particle Hydrodynamic (SPH) Method. *The International Journal of Advanced Manufacturing Technology* 83(5):985–994.
[50] Cao Y, Yin J, Ding W, Xu J (2021) Alumina Abrasive Wheel Wear in Ultrasonic Vibration-Assisted Creep-Feed Grinding of Inconel 718 Nickel-Based Superalloy. *Journal of Materials Processing Technology* 297:117241.
[51] Carreon AH, Funkenbusch PD (2019) Single-Grain Approach to Material Specific Dental Grinding-Force Equations. *Journal of Manufacturing Processes* 37:281–291.
[52] Chang H-C, Wang JJJ (2008) A Stochastic Grinding Force Model Considering Random Grit Distribution. *International Journal of Machine Tools and Manufacture* 48 (12):1335–1344.
[53] Chaudhari A, Sharma A, Awale AS, Khan Yusufzai MZ, Vashista M (2022) Modeling and Simulation Study of Dry Ultrasonic Vibration-Assisted Grinding of Tool Steel with Single Alumina Abrasive Grit. *Journal of Manufacturing Science and Engineering* 144(11):111001.
[54] Chen C, Tang J, Chen H, Zhu C (2017) Research About Modeling of Grinding Workpiece Surface Topography Based on Real Topography of Grinding Wheel. *The International Journal of Advanced Manufacturing Technology* 93 (5):2411–2421.
[55] Chen H, Tang J (2016) Influence of Ultrasonic Assisted Grinding on Abbott-Firestone Curve. *The International Journal of Advanced Manufacturing Technology* 86 (9):2753–2757.
[56] Chen S, Cheung BCF, Zhao C, Zhang F (2017) Simulated and Measured Surface Roughness in High-Speed Grinding of Silicon Carbide Wafers. *The International Journal of Advanced Manufacturing Technology* 91(1):719–730.
[57] Chen X, Mohammed A, Oluwajobi A (2012) Investigation of AE Features in Grinding. *Journal of Physics: Conference Series* 364(1):012090.
[58] Chen X, Öpöz TT, Oluwajobi A (2017) Analysis of Grinding Surface Creation by Single-Grit Approach. *Journal of Manufacturing Science and Engineering* 139 (12):121007.
[59] Chen X, Rowe W, Mills B, Allanson D (1998) Analysis and Simulation of the Grinding Process. Part IV: Effects of Wheel Wear. *International Journal of Machine Tools and Manufacture* 38:41–49.
[60] Cheng J, Gong YD (2014) Experimental Study of Surface Generation and Force Modeling in Micro-Grinding of Single Crystal Silicon Considering Crystallographic Effects. *International Journal of Machine Tools and Manufacture* 77:1–15.
[61] Cheng J, Yang Z, Wang C, Zhao L, Chen M, Wang J, Li Y, Xu Q, Liu Z, Xu H (2022) Effect of Scratches on the Damage Characteristics of Fused Silica Optics under Extremely-High Impact Load. *International Journal of Mechanical Sciences* 219:107099.
[62] Cheng J, Yin G, Wen Q, Song H, Gong Y (2015) Study on Grinding Force Modelling and Ductile Regime Propelling Technology in Micro Drill-Grinding of Hard-Brittle Materials. *Journal of Materials Processing Technology* 223:150–163.
[63] Christ M, Braun N, Neuffer J, Kempa-Liehr AW (2018) Time Series FeatuRe Extraction on Basis of Scalable Hypothesis Tests (tsfresh – a Python Package). *Neurocomputing* 307:72–77.
[64] D'Addona DM, Matarazzo D, Teti R, de Aguiar PR, Bianchi EC, Fornaro A (2017) Prediction of Dressing in Grinding Operation Via Neural Networks. *Procedia CIRP* 62:305–310.

Please cite this article as: P. Krajnik et al., Advances in modeling of fixed-abrasive processes, CIRP Annals - Manufacturing Technology (2024), https://doi.org/10.1016/j.cirp.2024.05.001

[65] Dai J, Ding W, Zhang L, Xu J, Su H (2015) Understanding the Effects of Grinding Speed and Undeformed Chip Thickness on the Chip Formation in High-Speed Grinding. *The International Journal of Advanced Manufacturing Technology* 81(5):995–1005.
[66] Dai J, Su H, Zhou W, Zhang Q, Zheng Y (2019) Experimental and Numerical Investigation on the Interference of Diamond Grains in Double-Grain Grinding Silicon Carbide Ceramics. *Journal of Manufacturing Processes* 44:408–417.
[67] de Oliveira Teixeira P, Brimmers J, Bergs T (2022) Consideration of Micro-Interaction in the Modeling of Generating Gear Grinding Processes. *Forschung im Ingenieurwesen* 86(3):639–647.
[68] de Payrebrune K, Kröger M (2017) Effects of the Grinding Wheel Eccentricity and Waviness on the Dynamics of Tool Grinding. *Applied Mechanics and Materials* 869:128–138.
[69] de Payrebrune KM, Kröger M (2011) Nonlinear Process Machine Interaction in Tool Grinding. *82nd Annual Meeting of the International Association of Applied Mathematics and Mechanics (GAMM)*, Graz, Austria, 927–930.
[70] Deichmueller M, Denkena B, de Payrebrune KM, Kröger M, Wiedemann S, Schröder A, Carstensen C (2012) Modeling of Process Machine Interactions in Tool Grinding. *Process Machine Interactions, Lecture Notes in Production Engineering, Berlin, Heidelberg, Germany*, 143–176.
[71] Denkena B, Boujnah H (2018) Feeling Machines for Online Detection and Compensation of Tool Deflection in Milling. *CIRP Annals* 67(1):423–426.
[72] Denkena B, Grove T, Behrens L, Müller-Cramm D (2020) Wear Mechanism Model for Grinding of PcBN Cutting Inserts. *Journal of Materials Processing Technology* 277:116474.
[73] Denkena B, Hollmann F (2013) *Process Machine Interactions*, Springer, Berlin, Heidelberg, Germany.
[74] Dereli T, Schmidt N, Furlan T, Holtermann R, Biermann D, Menzel A (2021) Simulation Based Prediction of Compliance Induced Shape Deviations in Internal Traverse Grinding. *Journal of Manufacturing and Materials Processing* 5(2):60.
[75] Devendiran S, Manivannan K (2013) Condition Monitoring on Grinding Wheel Wear Using Wavelet Analysis and Decision Tree C4.5 Algorithm. *International Journal of Engineering and Technology* 5:4010–4024.
[76] Di Ilio A, Paoletti A, D'Addona D (2009) Characterization and Modelling of the Grinding Process of Metal Matrix Composites. *CIRP Annals* 58(1):291–294.
[77] Dietz C (2017) *Numerische Simulation Des Kontinuierlichen Wälzschleifprozesses Unter Berücksichtigung Des Systems Maschine - Werkzeug - Werkstück*, Ph.D. Thesis, ETH Zürich, Switzerland.
[78] Dietz C, Wegener K, Thyssen W (2016) Continuous Generating Grinding: Machine Tool Optimisation by Coupled Manufacturing Simulation. *Journal of Manufacturing Processes* 23:211–221.
[79] Ding W, He W, Zhang H, Li Y (2022) Effect of Assembly Errors on Ground Tooth Surface Deviations for Large-Scale CNC Gear Profile Grinding Machines. *Machines* 10(2):111.
[80] Ding Z, Sun G, Guo M, Jiang X, Li B, Liang SY (2020) Effect of Phase Transition on Micro-Grinding-Induced Residual Stress. *Journal of Materials Processing Technology* 281:116647.
[81] Dittrich MA, Denkena B, Wichmann M (2021) Parametric Grinding Wheel Model for Material Removal Simulation of Tool Grinding Processes. *Procedia CIRP* 102:381–386.
[82] Doetz M, Dambon O, Klocke F, Faehnle O, Langenbach E (2018) Process Control in Ductile Mode Machining of Tungsten Carbide. *In: SPIE Optical Systems Design, Frankfurt, Germany*:1069210.
[83] Dokeroglu T, Deniz A, Kiziloz HE (2022) A Comprehensive Survey on Recent Metaheuristics for Feature Selection. *Neurocomputing* 494:269–296.
[84] Dornfeld DA, Lee Y, Chang A (2003) Monitoring of Ultraprecision Machining Processes. *The International Journal of Advanced Manufacturing Technology* 21(8):571–578.
[85] Drazumeric R, Badger J, Gustavsson T, Krajnik P (2022) Mechanics of Self-Rotating Double-Disc Grinding Process. *CIRP Annals* 71(1):309–312.
[86] Drazumeric R, Badger J, Klement U, Krajnik P (2018) Truing of Diamond Wheels – Geometry, Kinematics and Removal Mechanisms. *CIRP Annals* 67(1):345–348.
[87] Drazumeric R, Badger J, Krajnik P (2014) Geometric, Kinematical and Thermal Analyses of Non-Round Cylindrical Grinding. *Journal of Materials Processing Technology* 214(4):818–827.
[88] Drazumeric R, Badger J, Krajnik P (2017) Wheel Lift-Off in Creep-Feed Grinding: Thermal Damage, Power Surge, Chip Thickness and Optimisation. *International Journal of Abrasive Technology* 8:97.
[89] Drazumeric R, Badger J, Roininen R, Krajnik P (2020) On Geometry and Kinematics of Abrasive Processes: The Theory of Aggressiveness. *International Journal of Machine Tools and Manufacture* 154:103567.
[90] Drazumeric R, Krajnik P, Vrabic R, Meyer B, Butala P, Kosel F, Kopac J (2010) Modelling of Grinding Gap Macro Geometry and Workpiece Kinematics in Throughfeed Centreless Grinding. *Journal of Materials Processing Technology* 210(1):104–109.
[91] Drazumeric R, Roininen R, Badger J, Krajnik P (2018) Temperature-Based Method for Determination of Feed Increments in Crankshaft Grinding. *Journal of Materials Processing Technology* 259:228–234.
[92] Drucker DC, Prager W (1952) Soil Mechanics and Plastic Analysis or Limit Design. *Quarterly of Applied Mathematics* 10(2):157–165.
[93] Duan N, Yu Y, Wang W, Xu X (2017) Analysis of Grit Interference Mechanisms for the Double Scratching of Monocrystalline Silicon Carbide by Coupling the FEM and SPH. *International Journal of Machine Tools and Manufacture* 120:49–60.
[94] Eda H, Kishi K, Usui N, Ueno H, Kakino Y, Fujiwara A (1983) In-Process Detection of Grinding Burn by Means of Utilizing Acoustic Emission. *Journal of the Japan Society of Precision Engineering* 49(9):1257–1262.
[95] Eder SJ, Feldbauer G, Bianchi D, Cihak-Bayr U, Betz G, Vernes A (2015) Applicability of Macroscopic Wear and Friction Laws on the Atomic Length Scale. *Physical Review Letters* 115(2):025502.
[96] Esmaeili H, Adibi H, Rezaei SM (2021) Study on Surface Integrity and Material Removal Mechanism in Eco-Friendly Grinding of Inconel 718 Using Numerical and Experimental Investigations. *The International Journal of Advanced Manufacturing Technology* 112(5):1797–1818.
[97] Godoy Neto FR, Marchi M, Martins C, Aguiar PR, Bianchi E (2014) Monitoring of Grinding Burn by Ae and Vibration Signals. In: *Proceedings of the 6th International Conference on Agents and Artificial Intelligence (ICAART), Angers, France*, 272–279.
[98] Fabbro S, Afrasiabi M, Marra L, Kuffa M, Bambach M, Wegener K (2022) Experimental Study and Smoothed Particle Hydrodynamics Simulation of Synthetic Diamond Grit Scratching on Steel. *International Journal of Solids and Structures* 259:112038.
[99] Feng W, Yao B, Chen B, Zhang D, Zhang X, Shen Z (2015) Modeling and Simulation of Process-Machine Interaction in Grinding of Cemented Carbide Indexable Inserts. *Shock and Vibration* 2015:508181.
[100] Frerichs F, Sölter J, Lübben T, Brinksmeier E, Zoch H-W (2016) A Simulation Based Development of Process Signatures for Manufacturing Processes with Thermal Loads. *Procedia CIRP* 45:327–330.
[101] Fu D, Ding W, Miao Q, Xu J (2017) Simulation Research on the Grinding Forces and Stresses Distribution in Single-Grain Surface Grinding of Ti-6Al-4V Alloy When Considering the Actual Cutting-Depth Variation. *The International Journal of Advanced Manufacturing Technology* 91:3591–3602.
[102] Gao S, Yang C, Xu J, Su H, Fu Y (2018) Modelling and Simulation of Bore Diameter Evolution in Finish Honing. *Procedia Manufacturing* 26:462–468.
[103] Garcia M, Alvarez J, Pombo I, Barrenetxea D (2022) Rotary Dressing Model for Grinding Wheel Active Surface Prediction. *CIRP Annals* 71(1):297–300.
[104] Gerstgrasser M, Smolenicki D, Akbari M, Klippel H, Roelofs H, Cadoni E, Wegener K (2021) Analysis of Two Parameter Identification Methods for Original and Modified Johnson-Cook Fracture Strains, Including Numerical Comparison and Validation of a New Blue-Brittle Dependent Fracture Model for Free-Cutting Steel 50SiB8. *Theoretical and Applied Fracture Mechanics* 112:102905.
[105] Godino L, Pombo I, Girardot J, Sanchez JA, Iordanoff I (2020) Modelling the Wear Evolution of a Single Alumina Abrasive Grain: Analyzing the Influence of Crystalline Structure. *Journal of Materials Processing Technology* 277:116464.
[106] Goeldel B, El Mansori M, Dumur D (2012) Macroscopic Simulation of the Liner Honing Process. *CIRP Annals* 61(1):319–322.
[107] Goeldel B, El Mansori M, Dumur D (2013) Simulation of Roughness and Surface Texture Evolution at Macroscopic Scale During Cylinder Honing Process. *Procedia CIRP* 8:27–32.
[108] Graf W (2004) *Leitfaden Zahnflankenschleifen*, Winterthur Schleiftechnik AG, Winterthur, Switzerland.
[109] Graham W, Voutsadopoulos CM (1978) Fracture Wear of Grinding Wheels. *International Journal of Machine Tool Design and Research* 18(2):95–103.
[110] Greenwood GW, Johnson RH (1965) The Deformation of Metals under Small Stresses During Phase Transformation. *Proceedings of the Royal Society A: Mathematical, Physical and Engineering Sciences* 283(1394):403–422.
[111] Griffin J, Chen X (2009) Multiple Classification of the Acoustic Emission Signals Extracted During Burn and Chatter Anomalies Using Genetic Programming. *The International Journal of Advanced Manufacturing Technology* 45:1152–1168.
[112] Grimmert A, Wiederkehr P (2021) Experimental Study on Macroscopic Force Modelling for Surface Grinding Processes in Aerospace Industry. *Procedia CIRP* 101:146–149.
[113] Grimmert A, Wiederkehr P (2021) Macroscopic Process Simulation of Surface and Profile Grinding Processes Estimating Forces for the Production of Turbine Blades. *Procedia CIRP* 102:126–131.
[114] Gu P, Zhu C, Tao Z, Yu Y (2021) Micro-Removal Mechanism of High Volume Fraction SiCp/Al Composite in Grinding Based on Cohesive Theory. *The International Journal of Advanced Manufacturing Technology* 117(1):243–265.
[115] Guo B, Zhao Q (2015) Wheel Normal Grinding of Hard and Brittle Materials. *The International Journal of Advanced Manufacturing Technology* 79(5):873–880.
[116] Guo C, Campomanes M, McIntosh D, Becze C, Green T, Malkin S (2003) Optimization of Continuous Dress Creep-Feed Form Grinding Process. *CIRP Annals* 52 (1):259–262.
[117] Guo C, Campomanes M, McIntosh D, Becze C, Malkin S (2004) Model-Based Monitoring and Control of Continuous Dress Creep-Feed Form Grinding. *CIRP Annals* 53(1):263–266.
[118] Guo C, Ranganath S, McIntosh D, Elfizy A (2008) Virtual High Performance Grinding with Cbn Wheels. *CIRP Annals* 57(1):325–328.
[119] Guo C, Shi Z, Attia H, McIntosh D (2007) Power and Wheel Wear for Grinding Nickel Alloy with Plated CBN Wheels. *CIRP Annals* 56(1):343–346.
[120] Guo S, Lu S, Zhang B, Cheung CF (2022) Surface Integrity and Material Removal Mechanisms in High-Speed Grinding of Al/SiCp Metal Matrix Composites. *International Journal of Machine Tools and Manufacture* 178:103906.
[121] Hanchate A, Bukkapatnam STS, Lee KH, Srivastava A, Kumara S (2023) Explainable AI (XAI)-Driven Vibration Sensing Scheme for Surface Quality Monitoring in a Smart Surface Grinding Process. *Journal of Manufacturing Processes* 99:184–194.
[122] Handa D, Kumar S, Surendran S, Sooraj VS (2021) Simulation of Intermittent Grinding for Ti-6Al-4V with Segmented Wheel. *Materials Today: Proceedings* 44 (1):2537–2542.
[123] Hashimoto F (2017) Model Development for Optimum Setup Conditions that Satisfy Three Stability Criteria of Centerless Grinding Systems. *Inventions* 2(4):26.
[124] Hashimoto F (2020) The Design of an Infeed Cylindrical Grinding Cycle. *Inventions* 5(3):46.
[125] Hashimoto F (2020) Dynamic Rounding Stability in Through-Feed Centerless Grinding. *Inventions* 5(2):17.
[126] Hashimoto F, Gallego I, Oliveira JFG, Barrenetxea D, Takahashi M, Sakakibara K, Stålfelt H-O, Staadt G, Ogawa K (2012) Advances in Centerless Grinding Technology. *CIRP Annals* 61(2):747–770.
[127] Hashimoto F, Lahoti GD (2004) Optimization of Set-up Conditions for Stability of the Centerless Grinding Process. *CIRP Annals* 53(1):271–274.
[128] Hashimoto F, Yamaguchi H, Krajnik P, Wegener K, Chaudhari R, Hoffmeister H-W, Kuster F (2016) Abrasive Fine-Finishing Technology. *CIRP Annals* 65(2):597–620.
[129] Heinzel C, Grimme D, Moisan A (2006) Modeling of Surface Generation in Contour Grinding of Optical Molds. *CIRP Annals* 55(1):581–584.

Please cite this article as: P. Krajnik et al., Advances in modeling of fixed-abrasive processes, CIRP Annals - Manufacturing Technology (2024), https://doi.org/10.1016/j.cirp.2024.05.001

[130] Heinzel C, Kirsch B, Meyer D, Webster J (2020) Interactions of Grinding Tool and Supplied Fluid. *CIRP Annals* 69(2):624–645.
[131] Hensel A (1978) *Kraft- und Arbeitsbedarf bildsamer Formgebungsverfahren*, Deutscher Verlag für Grundstoffindustrie, Leipzig, Germany.
[132] Hiraizumi Y, Hirata K, Ohishi S (2019) Grinding Energy Distributions and Wear Behaviors of Grain Cutting Edges in CBN Deep Grinding. *International Journal of Automation Technology* 14(1):59–65.
[133] Holtermann R, Schumann S, Menzel A, Biermann D (2013) Modelling, Simulation and Experimental Investigation of Chip Formation in Internal Traverse Grinding. *Production Engineering* 7(2):251–263.
[134] Huang H, Li X, Mu D, Lawn BR (2021) Science and Art of Ductile Grinding of Brittle Solids. *International Journal of Machine Tools and Manufacture* 161:103675.
[135] Huang X, Chai Z, Ren X, Chen X (2023) A Modified Infrared Emissivity Model Accurately Determining Dynamic Temperatures for Belt Grinding Inconel 718. *Journal of Manufacturing Processes* 101:86–103.
[136] Hübner F, Klocke F, Brecher C, Löpenhaus C (2015) Development of a Cutting Force Model for Generating Gear Grinding. *In: ASME 2015 Power Transmission and Gearing Conference*, Boston, MA, USA.
[137] Huo FW, Guo DM, Feng G, Kang RK, Wang RL (2012) A New Kinematics for Ultra Precision Grinding of Conical Surfaces Using a Rotary Table and a Cup Wheel. *International Journal of Machine Tools and Manufacture* 59:34–45.
[138] Huo FW, Kang RK, Li Z, Guo DM (2013) Origin, Modeling and Suppression of Grinding Marks in Ultra Precision Grinding of Silicon Wafers. *International Journal of Machine Tools and Manufacture* 66:54–65.
[139] Ichida Y (2008) Mechanical Properties and Grinding Performance of Ultrafine-Crystalline CBN Abrasive Grains. *Diamond and Related Materials* 17(7):1791–1795.
[140] Jackson M (2007) Modelling of Fracture Wear in Vitrified CBN Grinding Wheels. *Journal of Achievements in Materials and Manufacturing Engineering* 24(1):230–236.
[141] Jaeger JC (1942) Moving Sources of Heat and the Temperature at Sliding Contacts. *Journal and Proceedings of the Royal Society of New South Wales* 76:203–224.
[142] Jiang S, Li T, Tan Y (2015) A DEM Methodology for Simulating the Grinding Process of SiC Ceramics. *Procedia Engineering* 102:1803–1810.
[143] Jiang S, Tang C, Li X, Tan Y, Peng R, Yang D, Liu S (2020) Discrete Element Modeling of the Machining Processes of Brittle Materials: Recent Development and Future Prospective. *The International Journal of Advanced Manufacturing Technology* 109(9):2795–2829.
[144] Johnson EC, Li R, Shih AJ (2008) Design of Experiments Based Force Modeling of the Face Grinding Process. *Transactions of NAMRI/SME* 36:241–248.
[145] Johnson GR, Cook WH (1985) Fracture Characteristics of Three Metals Subjected to Various Strains, Strain Rates, Temperatures and Pressures. *Engineering Fracture Mechanics* 21(1):31–48.
[146] Johnson GR, Holmquist TJ (1994) An Improved Computational Constitutive Model for Brittle Materials. *AIP Conference Proceedings* 309(1):981–984.
[147] Johnson GR, Holmquist TJ, Beissel SR (2003) Response of Aluminum Nitride (Including a Phase Change) to Large Strains, High Strain Rates, and High Pressures. *Journal of Applied Physics* 94:1639–1646.
[148] Jung J, Kim P, Kim H, Seok J (2015) Dynamic Modeling and Simulation of a Nonlinear, Non-Autonomous Grinding System Considering Spatially Periodic Waviness on Workpiece Surface. *Simulation Modelling Practice and Theory* 57:88–99.
[149] Kadivar M, Azarhoushang B, Klement U, Krajnik P (2021) The Role of Specific Energy in Micro-Grinding of Titanium Alloy. *Precision Engineering* 72:172–183.
[150] Kadivar M, Azarhoushang B, Krajnik P (2020) Modeling of Micro-Grinding Forces Considering Dressing Parameters and Tool Deflection. *Precision Engineering* 67:269–281.
[151] Kadivar M, Azarhoushang B, Shamray S, Krajnik P (2017) The Effect of Dressing Parameters on Micro-Grinding of Titanium Alloy. *Precision Engineering* 51:176–185.
[152] Karpuschewski B, Kinner-Becker T, Klink A, Langenhorst L, Mayer J, Meyer D, Radel T, Reese S, Sölter J (2022) Process Signatures–Knowledge-Based Approach Towards Function-Oriented Manufacturing. *Procedia CIRP* 108:624–629.
[153] Kassen G (1969) *Beschreibung der elementaren Kinematik des Schleifvorganges*, Ph.D. Thesis. RWTH Aachen University, Germany.
[154] Kaufmann T, Sahay S, Niemietz P, Trauth D, Maaß W, Bergs T (2020) AI-Based Framework for Deep Learning Applications in Grinding. *In: IEEE 18th World Symposium on Applied Machine Intelligence and Informatics (SAMI), Herľany, Slovakia*, 195–200.
[155] Kersting P, Joliet R, Kansteiner M (2015) Modeling and Simulative Analysis of the Micro-Finishing Process. *CIRP Annals* 64(1):321–324.
[156] Khellouki A, Rech J, Zahouani H (2010) The Effect of Lubrication Conditions on Belt Finishing. *International Journal of Machine Tools and Manufacture* 50:917–921.
[157] Kienzle O (1952) Die Bestimmung von Kräften und Leistungen an spanenden Werkzeugen und Werkzeugmaschinen. *Zeitschrift des Vereins Deutscher Ingenieure* 94(11):299–305.
[158] Kienzle O, Victor H (1957) *Spezifische Schnittkräfte bei der Metallbearbeitung*, *Werkstattstechnik und Maschinenbau*, 224–225.
[159] Klippel H, Suessmaier S, Röthlin M, Afrasiabi M, Pala U, Wegener K (2021) Simulation of the Ductile Machining Mode of Silicon. *The International Journal of Advanced Manufacturing Technology* 115:1565–1578.
[160] Kohls E, Heinzel C, Eich M (2021) Evaluation of Hardness and Residual Stress Changes of AISI 4140 Steel Due to Thermal Load During Surface Grinding. *Journal of Manufacturing and Materials Processing* 5(3):73.
[161] Krajnik P, Drazumeric R (2019) Method of Grinding a Workpiece and Method for Determining Processing Parameters, Patent, US10293453B2.
[162] Krajnik P, Drazumeric R, Badger J (2013) Optimization of Peripheral Non-Round Cylindrical Grinding via an Adaptable Constant-Temperature Process. *CIRP Annals* 62(1):347–350.
[163] Krajnik P, Drazumeric R, Badger J, Hashimoto F (2014) Cycle Optimization in Cam-Lobe Grinding for High Productivity. *CIRP Annals* 63(1):333–336.
[164] Krajnik P, Drazumeric R, Meyer B, Kopac J, Zeppenfeld C (2008) Simulation of Workpiece Forming and Centre Displacement in Plunge Centreless Grinding. *International Journal of Machine Tools and Manufacture* 48(7):824–831.
[165] Krajnik P, Hashimoto F, Karpuschewski B, da Silva EJ, Axinte D (2021) Grinding and Fine Finishing of Future Automotive Powertrain Components. *CIRP Annals* 70(2):589–610.
[166] Krajnik P, Kopac J, Sluga A (2005) Design of Grinding Factors Based on Response Surface Methodology. *Journal of Materials Processing Technology* : 629–636.
[167] Krajnik P, Roininen R, Drazumeric R (2018) Method of Grinding a Workpiece Having a Cylindrical Bearing Surface and Method for Determining Processing Parameters, Patent, EP3115149B1.
[168] Kuang W, Miao Q, Ding W, Zhao Y, Zhao Z (2021) Residual Stresses of Turbine Blade Root Produced by Creep-Feed Profile Grinding: Three-Dimensional Simulation Based on Workpiece-Grain Interaction and Experimental Verification. *Journal of Manufacturing Processes* 62:67–79.
[169] Kuffa M, Kuster F, Wegener K (2017) Stochastic Kinematic Process Model with an Implemented Wear Model for High Feed Dry Grinding. *Inventions* 2(4):31.
[170] Kuffa M, Züger S, Kuster F, Wegener K (2016) A Kinematic Process Model and Investigation of Surface Roughness for High Efficiency Dry Grinding. *Procedia CIRP* 46:636–639.
[171] Kurrewar H (2021) *Chemo-Mechanical Finishing of Silicon Nitride ($Si_3N_4$) Ball*, Chalmers University of Technology. Sweden Ms.C. Thesis.
[172] Kuschel S, Kolkwitz B, Sölter J, Brinksmeier E, Heinzel C (2016) Experimental and Numerical Analysis of Residual Stress Change Caused by Thermal Loads During Grinding. *Procedia CIRP* 45:51–54.
[173] Kwak J-S, Ha M-K (2004) Detection of Dressing Time Using the Grinding Force Signal Based on the Discrete Wavelet Decomposition. *The International Journal of Advanced Manufacturing Technology* 23(1):87–92.
[174] Lajmert P, Sikora M, Kruszynski B, Ostrowski D (2018) Application of Principal Component Analysis and Decision Trees in Diagnostics of Cylindrical Plunge Grinding Process. *Advances in Manufacturing, Lecture Notes in Mechanical Engineering*, Springer, Berlin, Heidelberg, Germany 707–716.
[175] Lawn BR, Swain MV (1975) Microfracture Beneath Point Indentations in Brittle Solids. *Journal of Materials Science* 10(1):113–122.
[176] Lee C-H, Jwo J-S, Hsieh H-Y, Lin C-S (2020) An Intelligent System for Grinding Wheel Condition Monitoring Based on Machining Sound and Deep Learning. *IEEE Access* 8:58279–58289.
[177] Li C, Piao Y, Meng B, Hu Y, Li L, Zhang F (2022) Phase Transition and Plastic Deformation Mechanisms Induced by Self-Rotating Grinding of GaN Single Crystals. *International Journal of Machine Tools and Manufacture* 172:103827.
[178] Li H, Prinz S, Liu Y, Mattfeld P, Shih AJ (2023) Experiment and Smooth Particle Hydrodynamic Modeling of Single-Grain Diamond Scribing of Silicon Carbide Fiber Reinforced Silicon Carbide (SiCf/SiC). *CIRP Annals* 72(1):263–266.
[179] Li H, Yu T, Zhu L, Wang W (2015) Analysis of Loads on Grinding Wheel Binder in Grinding Process: Insights from Discontinuum-Hypothesis-Based Grinding Simulation. *The International Journal of Advanced Manufacturing Technology* 78 (9):1943–1960.
[180] Li P, Chen S, Xiao H, Chen Z, Qu M, Dai H, Jin T (2020) Effects of Local Strain Rate and Temperature on the Workpiece Subsurface Damage in Grinding of Optical Glass. *International Journal of Mechanical Sciences* 182:105737.
[181] Liang SY, Hecker RL, Landers RG (2004) Machining Process Monitoring and Control: The State-of-the-Art. *Journal of Manufacturing Science and Engineering* 126 (2):297–310.
[182] Liao YS, Luo SY (1992) Wear Characteristics of Sintered Diamond Composite During Circular Sawing. *Wear* 157(2):325–337.
[183] Linke B (2008) Dressing Process Model for Vitrified Bonded Grinding Wheels. *CIRP Annals* 57(1):345–348.
[184] Linke B, Garretson I, Torner F, Seewig J (2017) Grinding Energy Modeling Based on Friction, Plowing, and Shearing. *Journal of Manufacturing Science and Engineering* 139(12):121009.
[185] Liu G, Dang J, Chen Y, Dong D, An Q (2019) Numerical and Experimental Investigation on Grinding-Induced Exit Burr Formation. *The International Journal of Advanced Manufacturing Technology* 103(5):2331–2346.
[186] Liu W, Deng Z, Shang Y, Wan L (2019) Parametric Evaluation and Three-Dimensional Modelling for Surface Topography of Grinding Wheel. *International Journal of Mechanical Sciences* 155:334–342.
[187] Liu Y, Li B, Wu C, Kong L, Zheng Y (2018) Smoothed Particle Hydrodynamics Simulation and Experimental Analysis of SiC Ceramic Grinding Mechanism. *Ceramics International* 44(11):12194–12203.
[188] Liu Y, Li B, Zheng Y, Shih A (2017) Experiment and Smooth Particle Hydrodynamics Simulation of Debris Size in Grinding of Calcified Plaque in Atherectomy. *CIRP Annals* 66(1):325–328.
[189] Lortz W, Govekar E (2021) Advanced Modelling for Grinding - from Friction to Ploughing and Dynamic Chip Formation with Temperatures. *Procedia CIRP* 102:79–84.
[190] Macerol N, Franca L, Attia H, Krajnik P (2022) A Lapping-Based Test Method to Investigate Wear Behaviour of Bonded-Abrasive Tools. *CIRP Annals* 71(1):305–308.
[191] Macerol N, Franca LFP, Drazumeric R, Krajnik P (2022) The Effects of Grit Properties and Dressing on Grinding Mechanics and Wheel Performance: Analytical Assessment Framework. *International Journal of Machine Tools and Manufacture* 180:103919.
[192] Macerol N, Franca LFP, Krajnik P (2020) Effect of the Grit Shape on the Performance of Vitrified-Bonded CBN Grinding Wheel. *Journal of Materials Processing Technology* 277:116453.
[193] Rush Machinery, 2022, Truing Editor. Accessed: 12 April 2024. Available at: https://rushmachinery.com/truing-parameters-calculator/.
[194] Mahata S, Shakya P, Babu NR (2021) A Robust Condition Monitoring Methodology for Grinding Wheel Wear Identification Using Hilbert-Huang Transform. *Precision Engineering* 70:77–91.
[195] Maier M, Rupenyan A, Bobst C, Wegener K (2020) Self-Optimizing Grinding Machines Using Gaussian Process Models and Constrained Bayesian

Please cite this article as: P. Krajnik et al., Advances in modeling of fixed-abrasive processes, CIRP Annals - Manufacturing Technology (2024), https://doi.org/10.1016/j.cirp.2024.05.001

Optimization. *The International Journal of Advanced Manufacturing Technology* 108(1):539–552.
[196] Malakizadi A, Gruber H, Sadik I, Nyborg L (2016) An FEM-Based Approach for Tool Wear Estimation in Machining. *Wear* 368-369:10–24.
[197] Malakizadi A, Mallipeddi D, Dadbakhsh S, M'Saoubi R, Krajnik P (2022) Post-Processing of Additively Manufactured Metallic Alloys – a Review. *International Journal of Machine Tools and Manufacture* 179:103908.
[198] Malakizadi A, Shi B, Hoier P, Attia H, Krajnik P (2020) Physics-Based Approach for Predicting Dissolution-Diffusion Tool Wear in Machining. *CIRP Annals* 69 (1):81–84.
[199] Malkin S, Cook NH (1971) The Wear of Grinding Wheels: Part 1-Attritious Wear, Transactions of the ASME. *Journal of Engineering for Industry* 82:1120–1128.
[200] Malkin S, Cook NH (1971) The Wear of Grinding Wheels: Part 2-Fracture Wear, Transactions of the ASME. *Journal of Engineering for Industry* 93:1129–1133.
[201] Malkin S, Guo C (2007) Thermal Analysis of Grinding. *CIRP Annals* 56 (2):760–782.
[202] Malkin S, Guo C (2008) *Grinding Technology: Theory and Application of Machining with Abrasives*, Industrial Press Inc, New York, USA.
[203] Malkin S, Murray T (1978) Mechanics of Rotary Dressing of Grinding Wheels, Transactions of the ASME. *Journal of Engineering for Industry* 100:95.
[204] Markopoulos AP, Savvopoulos IK, Karkalos NE, Manolakos DE (2015) Molecular Dynamics Modeling of a Single Diamond Abrasive Grain in Grinding. *Frontiers of Mechanical Engineering* 10(2):168–175.
[205] Marra L, Fabbro S, Kuffa M, Wegener K (2023) Geometric-Kinematic Model for Reinforced Concrete Core Drilling. *The International Journal of Advanced Manufacturing Technology* 125(7):3149–3158.
[206] Marshall ER, Shaw MC (1952) Forces in Dry Surface Grinding. *Transactions of the ASME* 74(1):51–58.
[207] Meng Q, Guo B, Zhao Q, Li HN, Jackson MJ, Linke BS, Luo X (2023) Modelling of Grinding Mechanics: A Review. *Chinese Journal of Aeronautics* 36(7):25–39.
[208] Merchant ME (1945) Mechanics of the Metal Cutting Process. I. Orthogonal Cutting and a Type 2 Chip. *Journal of Applied Physics* 16(5):267–275.
[209] Mihic S, Drazumeric R, Pusavec F, Krajnik P, Badger J (2017) The Use of Computational Fluid Dynamics in the Analysis of Fluid Flow and Thermal Aspects in Grinding. *Proceedings of the Institution of Mechanical Engineers, Part B: Journal of Engineering Manufacture* 231(12):2103–2111.
[210] Mirifar S, Kadivar M, Azarhoushang B (2020) First Steps through Intelligent Grinding Using Machine Learning via Integrated Acoustic Emission Sensors. *Journal of Manufacturing and Materials Processing* 4(2):35.
[211] Mouli DSB, Rameshkumar K (2020) Acoustic Emission-Based Grinding Wheel Condition Monitoring Using Decision Tree Machine Learning Classifiers. *Advances in Materials and Manufacturing Engineering*, Springer, 353–359.
[212] Nguyen D, Yin S, Tang Q, Son PX, Duc LA (2019) Online Monitoring of Surface Roughness and Grinding Wheel Wear When Grinding Ti-6Al-4V Titanium Alloy Using ANFIS-GPR Hybrid Algorithm and Taguchi Analysis. *Precision Engineering* 55:275–292.
[213] Oliver WF (2016) Process Optimization in Optical Fabrication. *Optical Engineering* 55(3):035106.
[214] Opitz H, Guhring K (1968) High Speed Grinding. *CIRP Annals* 16(2):61–73.
[215] Osa JL, Sánchez JA, Ortega N, Iordanoff I, Charles JL (2016) Discrete-Element Modelling of the Grinding Contact Length Combining the Wheel-Body Structure and the Surface-Topography Models. *International Journal of Machine Tools and Manufacture* 110:43–54.
[216] Pahlitzsch G, Helmerdig H (1943) Bestimmung und Bedeutung der Spandicke beim Schleifen. *Werkstatttechnik* 11(12):397–400.
[217] Pala U (2020) *Experimental Investigation and Modeling of Diamond Wire Sawing of Single-Crystal Silicon*, Ph.D. Thesis, ETH Zurich, Switzerland.
[218] Palanna R, Bukkapatnam S, Stan Settles F (2003) Model-Based Tampering for Improved Process Performance-An Application to Grinding of Shafts. *Journal of Manufacturing Processes* 5(1):24–32.
[219] Pan Y, Zhao Q, Guo B, Chen B, Wang J, Wu X (2020) An Investigation of the Surface Waviness Features of Ground Surface in Parallel Grinding Process. *International Journal of Mechanical Sciences* 170:105351.
[220] Pan Y, Zhou P, Yan Y, Agrawal A, Wang Y, Guo D, Goel S (2021) New Insights into the Methods for Predicting Ground Surface Roughness in the Age of Digitalisation. *Precision Engineering* 67:393–418.
[221] Pandiyan V, Shevchik S, Wasmer K, Castagne S, Tjahjowidodo T (2020) Modelling and Monitoring of Abrasive Finishing Processes Using Artificial Intelligence Techniques: A Review. *Journal of Manufacturing Processes* 57:114–135.
[222] Pazmiño T, Pombo I, Girardot J, Godino L, Sánchez JA (2023) Multiscale Simulation of Volumetric Wear of Vitrified Alumina Grinding Wheels. *Wear* 530-531:205020.
[223] Peklenik J (1957) *Ermittlung von geometrischen und physikalischen Kenngrößen für die Grundlagenforschung des Schleifens*, Ph.D. Thesis, RWTH Aachen University, Germany.
[224] Peklenik J (1964) Contribution to the Correlation Theory for the Grinding Process. *Journal of Engineering for Industry* 86(2):85–94.
[225] Pinto F, Vargas G, Wegener K (2008) Simulation for Optimizing Grain Pattern on Engineered Grinding Tools. *CIRP Annals* 57(1):353–356.
[226] Pohl M, Börret R (2016) Simulation of Mid-Spatials from the Grinding Process. *Journal of the European Optical Society - Rapid Publications* 11:16010.
[227] Qiu Y, Yin J, Cao Y, Ding W (2021) Generation Mechanism Modeling of Surface Topography in Tangential Ultrasonic Vibration-Assisted Grinding with Green Silicon Carbide Abrasive Wheel. *Proceedings of the Institution of Mechanical Engineers, Part B: Journal of Engineering Manufacture* 236(6-7):694–706.
[228] Rabiey M, Zhi Wei JL (2018) Simulation of Workpiece Surface Roughness after Flat Grinding by Electroplated Wheel. *Procedia CIRP* 77:303–306.
[229] Röthlin M (2019) *Meshless Software Tool to Simulate Metal Cutting Operations By Employing Contemporary Numerical Methods*, Ph.D. Thesis, ETH Zürich, Switzerland.
[230] Röthlin M, Klippel H, Afrasiabi M, Wegener K (2019) Meshless Single Grain Cutting Simulations on the GPU. *International Journal of Mechatronics and Manufacturing Systems* 12(3-4):272–297.
[231] Rowe WB, Barash MM (1964) Computer Method for Investigating the Inherent Accuracy of Centreless Grinding. *International Journal of Machine Tool Design and Research* 4(2):91–116.
[232] Rowe WB, Barash MM, Koenigsberger F (1965) Some Roundness Characteristics of Centreless Grinding. *International Journal of Machine Tool Design and Research* 5(4):203–215.
[233] Rowe WB, Jin T (2001) Temperatures in High Efficiency Deep Grinding (HEDG). *CIRP Annals* 50(1):205–208.
[234] Rowe WB, Koenigsberger F (1965) The "Work-Regenerative" Effect in Centreless Grinding. *International Journal of Machine Tool Design and Research* 4 (3):175–187.
[235] Rowe WB, Miyashita M, Koenig W (1989) Centreless Grinding Research and its Application in Advanced Manufacturing Technology. *CIRP Annals* 38(2):617–625.
[236] Rowe WB, Yan L, Inasaki I, Malkin S (1994) Applications of Artificial Intelligence in Grinding. *CIRP Annals* 43(2):521–531.
[237] Sachin Krishnan P, Rameshkumar K (2021) Grinding Wheel Condition Prediction with Discrete Hidden Markov Model Using Acoustic Emission Signature. *Materials Today: Proceedings* 46:9168–9175.
[238] Safarzadeh H, Leonesio M, Bianchi G, Monno M (2021) Roundness Prediction in Centreless Grinding Using Physics-Enhanced Machine Learning Techniques. *The International Journal of Advanced Manufacturing Technology* 112(3):1051–1063.
[239] Sauter E, Sarikaya E, Winter M, Wegener K (2021) In-Process Detection of Grinding Burn Using Machine Learning. *The International Journal of Advanced Manufacturing Technology* 115(7):2281–2297.
[240] Scheffler F (2019) *Zerspankräfte beim kontinuierlichen Wälzschleifen von Strinradverzahnungen*, Ph.D. Thesis, RWTH Aachen University, Germany.
[241] Schieber C, Hettig M, Zaeh MF, Heinzel C (2021) Evaluation of Approaches to Compensate the Thermomechanical Distortion Effects During Profile Grinding. *Procedia CIRP* 102:331–336.
[242] Setti D, Arrabiyeh PA, Kirsch B, Heintz M, Aurich JC (2020) Analytical and Experimental Investigations on the Mechanisms of Surface Generation in Micro Grinding. *International Journal of Machine Tools and Manufacture* 149:103489.
[243] Shi Z, Malkin S (2005) Wear of Electroplated CBN Grinding Wheels. *Journal of Manufacturing Science and Engineering* 128(1):110–118.
[244] Siebrecht T, Biermann D, Ludwig H, Rausch S, Kersting P, Blum H, Rademacher A (2014) Simulation of Grinding Processes Using Finite Element Analysis and Geometric Simulation of Individual Grains. *Production Engineering* 8(3):345–353.
[245] Simha CH (1998) *High Rate Loading of a High-Purity Ceramic - One-Dimensional Stress Experiments and Constitutive Modeling*, Ph.D. Thesis, The University of Texas in Austin, USA.
[246] Snoeys R, Peters J, Decneut A (1974) The Significance of Chip Thickness in Grinding. *CIRP Annals* 23(2):227–237.
[247] Spaminato A, Axinte DA (2017) On Modelling the Interaction between Two Rotating Bodies with Statistically Distributed Features: An Application to Dressing of Grinding Wheels. *Proceedings of the Royal Society A: Mathematical, Physical and Engineering Sciences* 473(2208):20170466.
[248] Stachurski W, Sawicki J, Krupanek K, Nadolny K (2019) Numerical Analysis of Coolant Flow in the Grinding Zone. *The International Journal of Advanced Manufacturing Technology* 104(5):1999–2012.
[249] Storchak M, Rupp Möhring, Stehle H-C (2019) Determination of Johnson–Cook Constitutive Parameters for Cutting Simulations. *Metals* 9:473.
[250] Sun J, Chen P, Qin F, An T, Yu H, He B (2018) Modelling and Experimental Study of Roughness in Silicon Wafer Self-Rotating Grinding. *Precision Engineering* 51:625–637.
[251] Tao H, Liu Y, Zhao D, Lu X (2022) Undeformed Chip Width Non-Uniformity Modeling and Surface Roughness Prediction in Wafer Self-Rotational Grinding Process. *Tribology International* 171:107547.
[252] Teixeira P, Brimmers J, Bergs T (2021) Investigation of Mechanical Loads Distribution for the Process of Generating Gear Grinding. *Journal of Manufacturing and Materials Processing* 5(1):13.
[253] Teti R, Mourtzis D, D'Addona DM, Caggiano A (2022) Process Monitoring of Machining. *CIRP Annals* 71(2):529–552.
[254] Tigerström L, Svahn O (1975) A Model for Determination of Number of Active Grinding Edges in Various Grinding Processes. *CIRP Annals* 24(1):271–275.
[255] Tönshoff HK, Peters J, Inasaki I, Paul T (1992) Modelling and Simulation of Grinding Processes. *CIRP Annals* 41(2):677–688.
[256] Tu L, Li J, Shi W (2020) Investigation on Experiment and Simulation of the Grinding Process of Cast Iron. *Proceedings of the Institution of Mechanical Engineers, Part C: Journal of Mechanical Engineering Science* 234(13):2653–2661.
[257] Urgoiti L, Barrenetxea D, Sánchez JA, Godino L (2021) Experimental Study of Thermal Behaviour of Face Grinding with Alumina Angular Wheels Considering the Effect of Wheel Wear. *CIRP Journal of Manufacturing Science and Technology* 35:691–700.
[258] Urgoiti L, Barrenetxea D, Sánchez JA, Lanzagorta JL (2020) Detailed Thermo-Kinematic Analysis of Face Grinding Operations with Straight Wheels. *Metals* 10 (4):524.
[259] Usui E, Shirakashi T, Kitagawa T (1978) Analytical Prediction of Three Dimensional Cutting Process-Part 3: Cutting Temperature and Crater Wear of Carbide Tool. *Journal of Engineering for Industry* 100(2):236–243.
[260] Varga M, Leroch S, Gross T, Rojacz H, Eder S, Grillenberger M, Rodriguez Ripoll M (2021) Scratching Aluminium Alloys – Modelling and Experimental Assessment of Damage as Function of the Strain Rate. *Wear* 476:203670.
[261] Vargas GE, Wegener K, Kuster F, Schroeter RB (2014) Simulation of the Hone Broaching Process with Diamond Tools. *Journal of the Brazilian Society of Mechanical Sciences and Engineering* 36(2):325–333.
[262] Vodenitcharova T, Borrero-López O, Hoffman M (2012) Mechanics Prediction of the Fracture Pattern on Scratching Wafers of Single Crystal Silicon. *Acta Materialia* 60:4448–4460.

Please cite this article as: P. Krajnik et al., Advances in modeling of fixed-abrasive processes, CIRP Annals - Manufacturing Technology (2024), https://doi.org/10.1016/j.cirp.2024.05.001

[263] Vodenitcharova T, Zhang L (2004) A New Constitutive Model for the Phase Transformations in Mono-Crystalline Silicon. *International Journal of Solids and Structures* 41:5411–5424.
[264] Wang J, Yu T, Ding W, Fu Y, Bastawros AF (2018) Wear Evolution and Stress Distribution of Single CBN Superabrasive Grain in High-Speed Grinding. *Precision Engineering* 54:70–80.
[265] Wang P, Wang B, Melkote S (2020) Modeling and Simulation of Phase Transformation and Crack Formation During Scribing of Mono-Crystalline Silicon. *International Journal of Mechanical Sciences* 175:105527.
[266] Wang T, Liu H, Wu C, Cheng J, Chen M (2020) Three-Dimensional Modeling and Theoretical Investigation of Grinding Marks on the Surface in Small Ball-End Diamond Wheel Grinding. *International Journal of Mechanical Sciences* 173:105467.
[267] Wang Z, Willett P, DeAguiar PR, Webster J (2001) Neural Network Detection of Grinding Burn from Acoustic Emission. *International Journal of Machine Tools and Manufacture* 41(2):283–309.
[268] Warnecke G, Zitt U (1998) Kinematic Simulation for Analyzing and Predicting High-Performance Grinding Processes. *CIRP Annals* 47(1):265–270.
[269] Warren Liao T (2010) Feature Extraction and Selection from Acoustic Emission Signals with an Application in Grinding Wheel Condition Monitoring. *Engineering Applications of Artificial Intelligence* 23(1):74–84.
[270] Webster J, Marinescu I, Bennett R, Lindsay R (1994) Acoustic Emission for Process Control and Monitoring of Surface Integrity During Grinding. *CIRP Annals* 43(1):299–304.
[271] Wegener K, Hoffmeister HW, Karpuschewski B, Kuster F, Hahmann WC, Rabiey M (2011) Conditioning and Monitoring of Grinding Wheels. *CIRP Annals* 60 (2):757–777.
[272] Weiß M, Klocke F, Wegner H (2012) Process Machine Interaction in Pendulum and Speed-Stroke Grinding. *Process Machine Interactions, Lecture Notes in Production Engineering*, Berlin, Heidelberg, Germany, 101–120.
[273] Werner G (1971) *Kinematik und Mechanik des Schleifprozesses*, Ph.D. Thesis, RWTH Aachen University, Germany.
[274] Werner G, Younis MA (1970) Darstellung der Schleifergebnisse mit Hilfe eines die Einstellgrößen zusammenfassenden Faktors. *Industrie-Anzeiger* 92(70-71):1663–1666.
[275] Wiederkehr P, Finkeldey F, Merhofe T (2021) Augmented Semantic Segmentation for the Digitization of Grinding Tools Based on Deep Learning. *CIRP Annals* 70(1):297–300.
[276] Wiederkehr P, Siebrecht T, Potthoff N (2018) Stochastic Modeling of Grain Wear in Geometric Physically-Based Grinding Simulations. *CIRP Annals* 67 (1):325–328.
[277] Wöste F, Siebrecht T, Fast M, Wiederkehr P (2019) Geometric Physically-Based and Numerical Simulation of NC-Grinding Processes for the Calculation of Process Forces. *Procedia CIRP* 86:133–138.
[278] Wuest T, Weimer D, Irgens C, Thoben K-D (2016) Machine Learning in Manufacturing: Advantages, Challenges, and Applications. *Production & Manufacturing Research* 4(1):23–45.
[279] Xiao G, Zhu B, Zhang Y, Gao H (2023) FCSNet: A Quantitative Explanation Method for Surface Scratch Defects During Belt Grinding Based on Deep Learning. *Computers in Industry* 144:103793.
[280] Yang CT, Shaw MC (1955) The Grinding of Titanium Alloys. *Transactions of the ASME* 77(5):645–654.
[281] Yang M, Li C, Zhang Y, Jia D, Zhang X, Hou Y, Li R, Wang J (2017) Maximum Undeformed Equivalent Chip Thickness for Ductile-Brittle Transition of Zirconia Ceramics under Different Lubrication Conditions. *International Journal of Machine Tools and Manufacture* 122:55–65.
[282] Yang Y, Liao Z, Wang Z (2022) Predictive Model of the Surface Topography for Compliant Grinding of Brittle Materials. *CIRP Annals* 71(1):465–468.
[283] Yang Z, Yu Z (2012) Grinding Wheel Wear Monitoring Based on Wavelet Analysis and Support Vector Machine. *The International Journal, Advanced Manufacturing Technology* 62(1):107–121.
[284] Yang Z, Yu Z (2013) Experimental Study of Burn Classification and Prediction Using Indirect Method in Surface Grinding of AISI 1045 Steel. *The International Journal of Advanced Manufacturing Technology* 68:2439–2449.
[285] Yang Z, Yu Z, Xie C, Huang Y (2014) Application of Hilbert-Huang Transform to Acoustic Emission Signal for Burn Feature Extraction in Surface Grinding Process. *Measurement* 47:14–21.
[286] Yen YC, Söhner J, Weule H, Schmidt J, Altan T (2002) Estimation of Tool Wear of Carbide Tool in Orthogonal Cutting Using FEM Simulation. *Machining Science and Technology* 6(3):467–486.
[287] Yiming M, Zhonghua Y, Zhensheng Y (2017) Numerical Investigation of the Evolution of Grit Fracture and its Impact on Cutting Performance in Single Grit Grinding. *The International Journal of Advanced Manufacturing Technology* 89 (9):3271–3284.
[288] Yin T, To S, Du H, Zhang G (2022) Effects of Wheel Spindle Error Motion on Surface Generation in Grinding. *International Journal of Mechanical Sciences* 218:107046.
[289] Yongcheng P, Zhao Q, Guo B, Chen B, Wang J (2020) Suppression of Surface Waviness Error of Fresnel Micro-Structured Mold by Using Non-Integer Rotation Speed Ratio in Parallel Grinding Process. *Micromachines* 11:652.
[290] Zahedi A, Azarhoushang B (2016) FEM Based Modeling of Cylindrical Grinding Process Incorporating Wheel Topography Measurement. *Procedia CIRP* 46:201–204.
[291] Zeng X, Xiong W, Zhang H, Li Y, Yuan S, Jin Z (2023) Research on the Consistency Model of Roundness Error in Journal Cylindrical Grinding with Random Parameters. *Precision Engineering* 82:270–280.
[292] Zhang B, Lu S, Rabiey M, Axinte D, Bleicher F (2023) Grinding of Composite Materials. *CIRP Annals* 72(2):645–671.
[293] Zhang L, Rowe BW (2020) Fluid Convection Models for Low-Temperature Grinding and Effect of Fluid Warming. *Journal of Manufacturing Science and Engineering* 143(2):021010.
[294] Zhang W, Subhash G (2001) An Elastic–Plastic–Cracking Model for Finite Element Analysis of Indentation Cracking in Brittle Materials. *International Journal of Solids and Structures* 38:5893–5913.
[295] Zhang Y, Zhu S, Zhao Y, Yin Y (2022) A Material Point Method Based Investigation on Crack Classification and Transformation Induced by Grit Geometry During Scratching Silicon Carbide. *International Journal of Machine Tools and Manufacture* 177:103884.
[296] Zhang Z, Yao P, Li X, Wang J, Huang C, Zhu H, Zou B, Liu H (2020) Grinding Performance and Tribological Behavior in Solid Lubricant Assisted Grinding of Glass-Ceramics. *Journal of Manufacturing Processes* 51:31–43.
[297] Zheng Y, Liu Y, Liu Y, Shih A (2019) Multi-Grain Smoothed Particle Hydrodynamics and Hertzian Contact Modeling of the Grinding Force in Atherectomy. *Journal of Manufacturing Science and Engineering* 141(4):041015.
[298] Zhu T, Cai M, Gong Y, Gao X, Yu N, Li X (2022) Study on Chip Formation in Grinding of Nickel-Based Polycrystalline Superalloy GH4169. *The International Journal of Advanced Manufacturing Technology* 121(1):1135–1148.
[299] Zhu W-L, Jain C, Han Y, Beaucamp A (2021) Predictive Topography Model for Shape Adaptive Grinding of Metal Matrix Composites. *CIRP Annals* 70(1):269–272.
[300] Zhuang X, Ma Y, Zhao Z (2019) Fracture Prediction under Nonproportional Loadings by Considering Combined Hardening and Fatigue-Rule-Based Damage Accumulation. *International Journal of Mechanical Sciences* 150:51–65.

Please cite this article as: P. Krajnik et al., Advances in modeling of fixed-abrasive processes, CIRP Annals - Manufacturing Technology (2024), https://doi.org/10.1016/j.cirp.2024.05.001